The crevice model of bubble nucleation

Anthony A. Atchley
Department of Physics, Naval Postgraduate School, Monterey, California 93943

Andrea Prosperetti
Department of Mechanical Engineering, Johns Hopkins University, Baltimore, Maryland 21218

(Received 19 September 1988; accepted for publication 17 May 1989)

The crevice model for heterogeneous nucleation of bubbles in water in response to a decreasing liquid pressure is studied. The model neglects gas-diffusion effects and is therefore more suited for acoustic than for flow cavitation. It is argued that previous work has overlooked the essential requirement of *unstable* growth of the interface in the crevice. As a consequence, the available results are incorrect in some cases. Another feature of the model which is considered is the process by which the interface moves out of the crevice. It is concluded that, depending on circumstances, the conditions for this step may be more stringent than those for the initial expansion of the nucleus inside the crevice. Some numerical examples are given to illustrate the complex behavior of nuclei, depending of geometrical parameters, gas saturation, contact angles, and other quantities.

PACS numbers: 43.35.Ei, 43.30.Nb

INTRODUCTION

The nature of nucleation and cavitation processes in water has been investigated in the literature since the midnineteenth century.[1–30] A basic conclusion drawn from these studies is that only in rare instances, if at all, does nucleation occur within the bulk of the homogeneous liquid. In order to explain the results of the experiments, it has been necessary to postulate the existence of inhomogeneities in the liquid on which the observed nucleation originated. These inhomogeneities, be they free bubbles, dirt particles, clusters of organic or ionic molecules, or due to a cosmic ray or other form of radiation, have been given the generic name of *cavitation nuclei*. In general (excluding radiation-induced cavitation), cavitation nuclei are long lived and are comprised at least in part by a volume of gas.[16] The first of these characteristics excludes free bubbles from the list of nucleation candidates for cavitation in undisturbed liquids which have been left standing for some time. Free bubbles will quickly dissolve in liquids that are not supersaturated with gas,[31] and bubbles having radii of less than a critical value will dissolve even in a supersaturated liquid.[9,31] Bubbles of larger than critical radius will grow in a supersaturated liquid. In either case, free bubbles are unstable and the liquid will soon be free of them. This instability must be eliminated by any plausible nucleation model. Of the many proposed nucleation models, the two most successful ones are the varying-permeability model[26,27,29] and the crevice model.[6,16,20,25]

The varying-permeability model, which employs a skin of surface-active molecules to stabilize the nucleus, has been applied mainly to bubble formation in supersaturated liquids.[26] The model is plausible and in fact the proposed nuclei have been observed microscopically.[29] The crevice model postulates that small pockets of gas are stabilized at the bottom of cracks or crevices found on hydrophobic solid impurities in the liquid. This model has been applied to various types of cavitation, but its greatest success appears to be in the explanation of acoustic cavitation processes.[16,20,25] It is fair to say that, in the light of present knowledge, there are insufficient elements to decide between these two models, which, in fact, are not mutually exclusive. Both kinds of nuclei may exist in nature with a prevalence of one form or the other, depending on the situation.

The first quantitative application of the crevice model was made by Harvey[6] in a study of bubble formation in animals. Strasberg[16] was the first to apply it to acoustic cavitation and was able to explain the dependence of the acoustic cavitation threshold on the gas content and prepressurization of the liquid. The acoustic cavitation threshold is the pressure amplitude which must be applied to a liquid in order to cause the onset of cavitation. Apfel[20] extended Strasberg's results to include the threshold's dependence on vapor pressure, temperature, and crevice size. Crum[25] further extended the crevice model to include the effect of surface tension on contact angles.

In this paper we reexamine the crevice model and show that the nucleation criterion used by previous investigators is incomplete in that it does not include the essential requirement of mechanically unstable growth of the nucleus as the pressure falls. This condition can lead to substantial differences in some cases, particularly at the higher gas concentrations. We also consider the model in parameter ranges in which it has never been studied before. Finally, we include an analysis of the fate of the nucleus when its surface reaches the crevice mouth. In some cases, the growth past this point may require lower absolute pressures than those necessary for the initial growth. In these cases too the cavitation threshold that we calculate is at variance with that predicted by the previous versions of the crevice model.

From our study it appears that, depending on the parameter values associated with each nucleus, the crevice model can exhibit a bewildering variety of behaviors, which does not seem to have been appreciated before. We believe that many of the earlier conclusions on its physical implica-

 0001-4966/89/091065-20$00.80

tions and predictions must be revised, and that the current understanding of the model is superficial, and possibly misleading.

This paper is planned as follows. In Sec. I the mechanism of nucleus stabilization in a solid crevice is reviewed. The essential idea on which the entire study is based, namely, the loss of mechanical stability, is described and justified in Sec. II, which also contains some considerations on the expected range of applicability of the model. In Sec. III the concepts of mechanical stability and unstable growth are illustrated in the simplest context, that of the free spherical bubble. Section IV summarizes some geometrical formulas, and Secs. V and VI are devoted to the investigation of the crevice model, in the parameter range considered by other authors, and in other ranges. Section VII studies the mechanism by which the interface can get out of the crevice. Section VIII contains the results of a preliminary parametric study, while our conclusions are drawn in Sec. IX.

I. STABILIZATION OF THE NUCLEUS

The amount of gas dissolved in the neighborhood of a liquid surface in contact with a gas at a partial pressure p_g is determined by Henry's law:

$$c = K(T)p_g, \tag{1}$$

which c is the concentration and $K(T)$ is a function of temperature only. This relation can be used to convert concentrations into pressures, and we define the *gas tension* G corresponding to a given concentration c as

$$G = c/K(T). \tag{2}$$

Referring to Fig. 1, consider a closed container partially filled with liquid. The space above the liquid contains vapor and another gas at a partial pressure p_g. Neglecting hydrostatic effects, the total pressure in this space, $p_g + p_v$, must evidently equal the pressure in the liquid p_L so that, by (1),

$$c_s = K(T)(p_L - p_v). \tag{3}$$

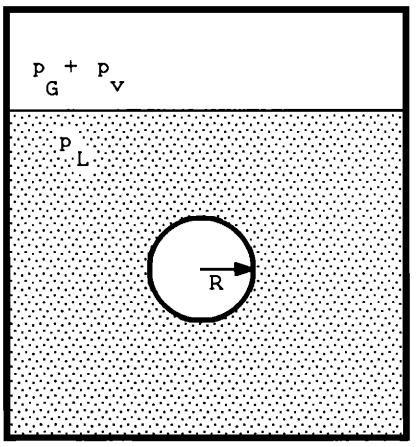

FIG. 1. Diagram of a closed container partially filled with a liquid. The pressure in the space above the liquid is equal to the sum of the vapor pressure p_v and the partial pressure of the gas dissolved in the liquid p_g. Within the liquid is a spherical bubble of radius R.

At equilibrium, the liquid is uniformly saturated with gas at this saturation concentration c_s.

Consider now a free bubble in the liquid, and let p_G be the partial pressure of the gas inside it. The balance of normal stresses across the bubble interface is expressed by Laplace's equation:

$$p_G + p_v = p_L + \sigma C, \tag{4}$$

where σ is the surface-tension coefficient and C is the curvature, equal to $2/R$ for a sphere of radius R. In the sequel we shall refer to σC as the Laplace pressure.

We consider C positive when the radius of curvature lies on the gas side of the interface. Since $\sigma C > 0$ for a spherical bubble, $p_G > p_L - p_v$, and therefore, by (1), the concentration of gas dissolved near the bubble surface exceeds the concentration in the liquid given by (3). A concentration gradient therefore exists in the system, which leads to the dissolution of the bubble by diffusion. While other models need the effect of surface tension to be counterbalanced to achieve stability of the nucleus, it is characteristic of the crevice model that stabilization is attained because of it, as we now show.

Water normally contains a large number of suspended solid impurities which, examined by means of a scanning electron microscope, reveal a very irregular surface deeply marked by grooves and pits.[25] The surface of these impurities is frequently hydrophobic either because the material itself is, or because hydrophobic organic contaminants have been adsorbed on it. As a consequence, when the impurity comes into contact with the liquid, some gas remains entrapped at the bottom of the narrowest surface crevices. The difference with the free-bubble case is that, due to the presence of the solid, the free surface of the liquid trapping the gas need not be convex towards the liquid; that is, C need not be positive. The gas concentration in the neighborhood of the surface can therefore be equal to c_s as everywhere else in the liquid, and the nucleus can last indefinitely. More interestingly, stability of the nucleus can also be achieved in an undersaturated liquid, for which $c < c_s$. For this purpose it is sufficient that the liquid surface be convex towards the gas, so that the curvature C in (4) becomes negative (Fig. 2). In fact, if the crevice is so narrow as to allow a sufficiently large and negative curvature, equilibrium can be attained with no gas at all, the difference between p_L and p_v being completely balanced by the surface tension effect.

For simplicity, following previous treatments of the crevice model, we shall assume that the crevice is conical in shape with a half-angle aperture β (Fig. 2). Idealizing somewhat the initial filling of the crevice (Fig. 3), we conclude that only crevices such that

$$\alpha_A > \text{const} \times \beta, \tag{5}$$

where α_A is the advancing contact angle, can entrap air. The constant equals 2 for a wedge-shaped crevice, and can be expected to be of order 1 for the more complicated conical shape. At equilibrium, the free surface forms with the solid an angle α (measured through the liquid, Fig. 2) which cannot exceed α_A nor be smaller than α_R, the receding contact angle:

$$\alpha_R \leqslant \alpha \leqslant \alpha_A. \tag{6}$$

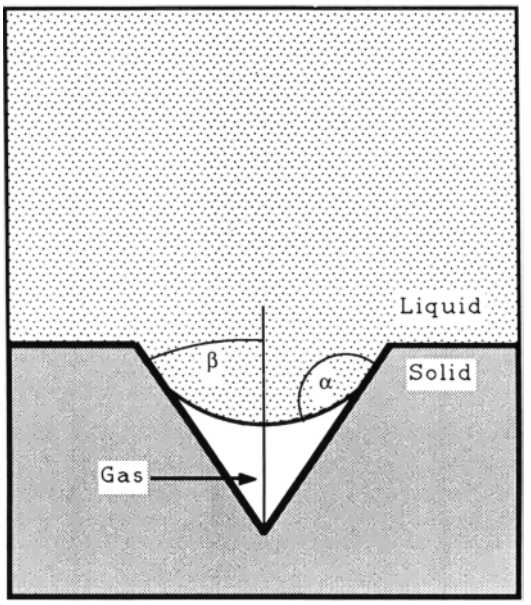

FIG. 2. The idealized model of a nucleus considered in this paper consists of a conical crevice of half-angle β in a hydrophobic solid. The contact angle α is the angle, measured in the liquid, which the liquid–gas interface makes with the solid. It must satisfy the relationship $\alpha_R \leqslant \alpha \leqslant \alpha_A$, where α_R is the receding contant angle and α_A is the advancing contact angle.

This relation has already some consequences for the stability of nuclei. For example, in the case of a saturated liquid, the interface must be flat so that $\alpha = \beta + \frac{1}{2}\pi$, and β must be such that (6) is satisfied. In a saturated or undersaturated liquid, if $\alpha_A < \beta + \frac{1}{2}\pi$, the interface will spontaneously move towards the bottom of the crevice, causing the complete dissolution of the gas. In a supersaturated liquid, on the other hand, such nuclei can be stable. In this case, however, if the other inequality is violated and $\alpha_R > \beta + \frac{1}{2}\pi$, the interface will spontaneously recede drawing gas from the solution into the nucleus, which will then slowly evolve into a gas bubble. It may be noted that, if the contact angle did not exhibit any hysteresis (i.e., if $\alpha_A = \alpha_R$), only nuclei with the sharply

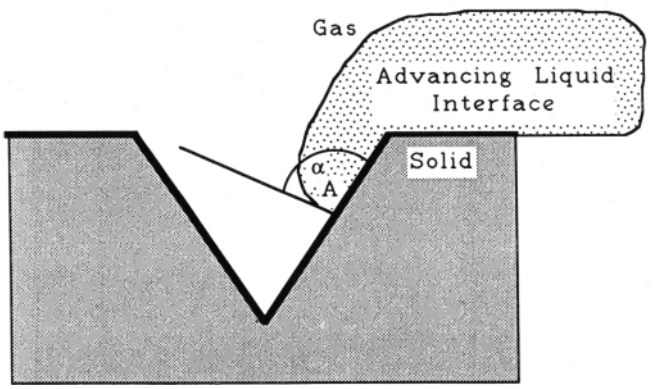

FIG. 3. Illustration of the initial filling of a crevice. The liquid surface advances at the advancing contact angle α_A.

defined aperture $\beta = \alpha_R - \pi/2 = \alpha_A - \pi/2$ could be stable in a saturated liquid. In this case, since presumably there is only a limited number of such nuclei, cavitation would be a rather infrequent event, in contrast with experience. This remark seems to indicate that the mechansim responsible for contact angle hysteresis works also on the submicrometer scale of the nuclei.

In general, the value of α and the penetration of the liquid into the crevice depend on the past history of the system. If, for example, the liquid is initially saturated and then progressively degassed, the liquid surface starts out as a plane ($\alpha = \beta + \pi/2$) and becomes more and more convex towards the gas. With continued degassing, the gas tension in the liquid G reaches a value G_A such that $\alpha = \alpha_A$. When G falls below G_A, the whole interface starts moving deeper towards the apex of the crevice so as to make the curvature more negative, but always maintaining $\alpha = \alpha_A$. An entirely similar process takes place when the liquid pressure p_L is increased, as in the deactivation of nuclei by prepressurization. This can be seen by noting that, for a fixed gas content of the liquid, an increase in the static pressure is equivalent to a decrease of the gas content with respect to the saturation level, as is evident from (3). Upon restoring the pressure to normal level, or increasing the gas content of the liquid, equilibrium is attained with $\alpha \leqslant \alpha_A$.

II. THE NUCLEATION EVENT

In acoustic cavitation a nucleation event consists of the formation of a detectable cavity from a nucleus during the expansion phase of the sound field. Although the detection of the cavity depends to some extent upon the sophistication of the means by which it is effected, for it to be possible, in most circumstances the volume of the nucleus must increase by one or more orders of magnitude. This remark shows that the nucleation event cannot be a volume increase caused, according to the gas law, by the fall of the liquid pressure during the expansion phase of the acoustic wave. Indeed, if this were the case, the inverse proportionality of volume to pressure would lead one to expect, in marked contrast with experience, cavitation thresholds of the order of tens of bars. Rather, as was first recognized by Blake,[8,9] and as will be seen below, another mode of cavity growth exists which is caused by the loss of mechanical stability of the balance of forces which determines the instantaneous volume of the nucleus. The cavity that forms in these circumstances is very much larger than the original nucleus and would, in fact, grow indefinitely if other effects (latent heat, phase reversal of the acoustic pressure, buoyancy, boundaries, and others) did not interfere.

It is in the explicit recognition of this fact that our study departs significantly from that of previous authors. Indeed, in earlier treatments of the crevice model, the cavitation threshold was taken to be the value of the liquid pressure at which the contact angle α at the liquid–solid–gas line reaches the receding value α_R. The justification given for this criterion was that, once the interface has reached α_R, any subsequent interfacial motion would decrease the curvature, resulting in a smaller Laplace pressure. This decrease in the Laplace pressure would reduce opposition to growth

even further and make it possible for the nucleus to expand under the action of the internal pressure $p_G + p_v$. This conceptual model, however, overlooks the fact that the motion of the interface causes *both* the Laplace pressure σC *and* the gas pressure p_G to decrease. If the gas pressure decreases faster than the Laplace pressure, the interface will recede relatively slowly and this motion will be arrested as soon as the liquid pressure stops falling. In other words, the system evolves quasistatically through a sequence of equilibrium configurations. On the contrary, if the Laplace pressure decreases *faster* than the gas pressure, it is evident that the situation is mechanically unstable and a rapid growth will take place.

It is clear from these considerations that the diffusion of gas in or out of the nucleus will have an important effect. If the diffusion is rapid enough to cause the partial gas pressure to fall slower than the Laplace pressure, the earlier treatments of this problem would be substantially adequate. In the opposite case, which is the one that we consider in this paper, where the gas content of the cavity is taken to remain constant, the differences between the two approaches can be important. Unfortunately, the diffusion of gas into a nucleus is a very complex problem about which very little is known. For instance, in view of the large differences in geometry and fluid dynamics, it is by no means clear that the available treatments of rectified diffusion for a free cavity bear much relevance to the case of a cavity trapped in a crevice. Perhaps, it is safe to say that our conclusions have a greater relevance at the higher frequencies of acoustic cavitation (hundreds of kHz–MHz range) where gas diffusion is expected to be less effective. Their relevance at lower frequencies and for flow cavitation remains to be established. The same argument leads one to expect that in the case of boiling, where the internal pressure in the nucleus is contributed mainly by the vapor with only a small effect of permanent gases, the earlier approaches would adequately capture the essence of the physical process of nucleation.

Mathematically, the situation that we describe is characterized by the instability of the equilibrium solution. When this solution is slightly perturbed, the collapsing forces, i.e., surface tension and liquid pressure, are insufficiently strong to balance the expanding forces, i.e., vapor and gas pressures. Therefore, in the following, we take the point of view that the (first) cavitation threshold is the absolute liquid pressure at which the interface loses mechanical stability *and* $\alpha = \alpha_R$. For those cases in which mechanical stability is lost before $\alpha = \alpha_R$ (i.e., the interface would move out unstably if the line of contact were free), our threshold criterion coincides with the one adopted by previous authors. If, however, when $\alpha = \alpha_R$ the configuration is stable, our criterion will predict cavitation to occur at a lower absolute pressure or, equivalently, at a higher value of the acoustic pressure amplitude. It may be said that, according to the present model, nucleation is *triggered* by a pressure decrease but, once initiated, would proceed independently of the pressure, provided the pressure remained below the threshold.

Another important aspect of the process, which apparently has been overlooked by previous authors, is the growth of the nucleus when its surface reaches the crevice mouth. The same requirement of instability applies to this stage which, as will be shown, may in fact require lower absolute pressures. For this reason we distinguish between the *first* threshold, defined above, which is the pressure necessary to cause the initital unstable motion of the contact line in the crevice, and the *second* threshold, which is that required for the unstable growth out of the crevice. The actual threshold at which a macroscopically detectable cavity is formed will correspond to the most stringent of these two criteria. It should also be noted that all these considerations refer to a single nucleus, and it is therefore unclear to what extent they can be applied to cavitation prediction in a liquid which would normally contain a wide variety of nuclei. Until a better feeling can be gained for the characteristics of the population of these nuclei, our results do not seem to be able to be turned into quantitative predictions of experimental cavitation thresholds.

In the preceding considerations we have only mentioned acoustic cavitation. However, with a suitable adjustment of the interpretation of the equations, the analysis of the following sections should also be valid for flow cavitation as well as boiling and gas supersaturation of the liquid, although, as already remarked, our results may not be as relevant in these cases.

III. FREE BUBBLE

In the following we shall make use repeatedly of an argument which is best illustrated with reference to a free spherical gas bubble. Hence, we introduce the notion of critical radius and mechanical instability in this context, although, as was remarked earlier, a free bubble cannot represent a viable model of cavitation nuclei.

By use of the perfect gas law, the equilibrum equation (4) becomes, for the case of a sphere of radius R,

$$3nBT/4\pi R^3 + p_v = p_L + 2\sigma/R, \tag{7}$$

where B is the universal gas constant, T is the absolute temperature of the gas, and n is the number of moles of gas in the bubble. This relation may be interpreted by saying that, at equilibrium, the expanding forces on the left-hand side (gas and vapor pressure) are balanced by the collapsing forces on the right-hand side (liquid and Laplace pressure). The character of the equilibrium described by (7) can be examined with reference to Fig. 4 in which, here as in the following, the thick line represents the left-hand side (expanding forces), while the thin lines show the right-hand side for three different values of p_L. For the largest value of p_L shown (line a) the thick and thin line cross for one value of R, which is thus the only solution of (7). If the radius undergoes a slight increase beyond this value, it is seen from the figure that the collapsing forces (thin line) are larger than the expanding forces, so that the radius will return to the original value. Conversely, a small decrease leads to a preponderance of the expanding forces and to a radius increase. This equilibrium configuration is therefore stable, and it is easy to see that this is the case as long as $p_L > p_v$. The argument given can be expressed formally by stating that the equilibrium is stable when, at the equilibrium point, the (negative) rate of change

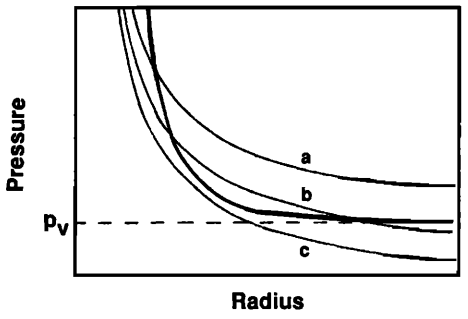

FIG. 4. Graph of the left-hand side (thick line) and the right-hand side (thin lines) of Eq. (7) versus radius for three values of p_L: line a—greater than p_v; line b—p_L slightly less than p_v; line c—p_L much less than p_v. Equation (7) can have one stable solution (line a), one stable and one unstable solution (line b), or no solutions (line c).

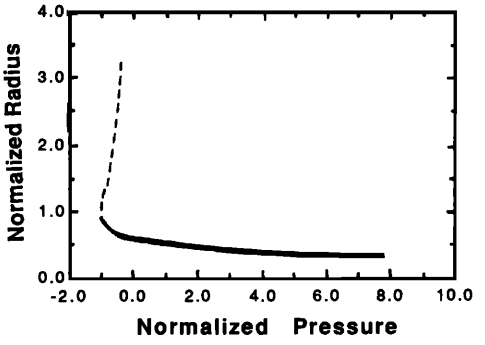

FIG. 5. Graph of the radius (normalized to R_c) vs $p_L - p_v$ (normalized to $p_v - p_{Lc}$) showing the equilibrium solutions of Eq. (7). The solid line represents the stable branch of solutions, while the dashed line represents the unstable branch.

of the collapsing forces is larger than that of the expanding forces:

$$\frac{d}{dR}\left(p_v + \frac{3nBT}{4\pi R^3}\right) < \frac{d}{dR}\left(p_L + \frac{2\sigma}{R}\right). \tag{8}$$

When p_L is somewhat below p_v (line b), there are two roots of (7). The same argument used above shows the root with the smaller radius to be stable, while the larger one is unstable. Indeed, if the radius is slightly increased beyond this value, the expanding forces dominate and cause an unstable growth of the bubble. Conversely, if the radius is slightly decreased, the bubble shrinks under the action of the collapsing forces until its radius takes on the smaller, stable equilibrum value. The same conclusion can be reached by use of the stability criterion (8). Finally, when the liquid pressure is much lower than p_v (line c), no solutions of (7) exist, the expanding forces always dominate, and the bubble grows without bound. The transition between these two regimes occurs when the two roots merge into one, at which point the curves are therefore tangent and (8) holds with an equal sign. Carrying out the differentiation indicated in this equation and solving for R, we find

$$R_c = (9nBT/8\pi\sigma)^{1/2}, \tag{9}$$

or using (7),

$$R_c = \tfrac{4}{3}\sigma/(p_v - p_{L,c}). \tag{10}$$

This *critical radius* R_c represents the largest possible radius that a bubble containing n moles of gas at a temperature T can have at equilibrium. It should be noted that the second expression (10) given for this quantity, although frequently quoted, is really an equation for the critical pressure $p_{L,c}$ rather than for the critical radius, the proper expression of which is (9). The results of this analysis are summarized in Fig. 5 in which the stable (continuous line) and the unstable (dashed line) solutions of (7) (i.e., the intersection points of the curves in Fig. 4), nondimensionalized by R_c, are plotted against $p_L - p_v$, nondimensionalized with respect to $p_v - p_{L,c}$.

To avoid confusion, it may be noted that the critical pressure is the pressure required for a bubble starting with a radius $R < R_c$ to expand to the value R_c. This remark explains why $p_{L,c} \to \infty$ *as* $n \to 0$, i.e., for a pure vapor bubble. This fact is at first sight perplexing since one does not expect that an infinite tension would be needed to promote the growth of a vapor bubble. Such a conclusion would, however, be false. A bubble containing little or no gas would have a radius close to

$$R = 2\sigma/(p_v - p_L).$$

It is seen from (8) that this value corresponds to the unstable solution of (7), and in agreement with the previous analysis, the bubble would therefore spontaneously expand or collapse as is well known. For small n the stable branch of the solutions of (7) is

$$R = 3^{-1/2}R_c\left(1 + \frac{p_v - p_L}{3^{1/2}4\sigma}R_c + O(n)\right),$$

with R_c given by (9) and therefore very small. What the results (9) and (10) imply in this case is only that a very large tension would be needed to expand such a small bubble from a radius *smaller* than the critical radius up to the critical radius. This very large tension is essentially that needed for homogeneous nucleation.

IV. CREVICE GEOMETRY

We collect in this section some geometrical formulas which will be referred to repeatedly in the following.

As already stated, we shall make use of an idealized nucleus having a conical shape of semiaperture β (Fig. 2). The radius of the crevice mouth is denoted by a_m, and the radius of the generic ring of contact by a. In this idealized geometry the liquid surface is a spherical segment of radius R making an angle of contact α (measured in the liquid, Fig. 2) with the cone wall. The relation between the radius of the ring of contact and R is given by

$$a = R\,|\cos(\alpha - \beta)|. \tag{11}$$

The volume of the portion of the cone of base a is

$$V_c = \tfrac{1}{3}\pi a^3 \cot\beta. \tag{12}$$

By combining this with the volume of a spherical segment, we can write down the volume occupied by the gas in each one of the possible configurations shown in Fig. 6. When the interface is concave towards the apex and either $\beta < \alpha$ [Fig. 6(a)] or $\alpha < \beta$ [Fig. 6(b)], this volume is

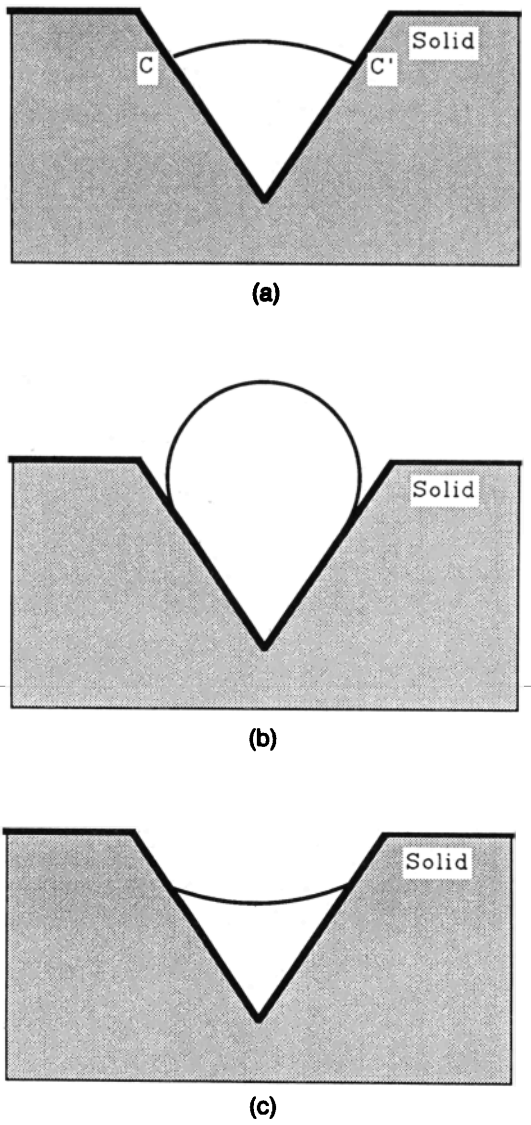

FIG. 6. Diagram showing the three possible configurations for the contact line CC' inside the crevice: (a) $\beta \leqslant \alpha \leqslant \pi/2 + \beta$; (b) $0 \leqslant \alpha \leqslant \beta$; (c) $\pi/2 + \beta \leqslant \alpha \leqslant \pi$.

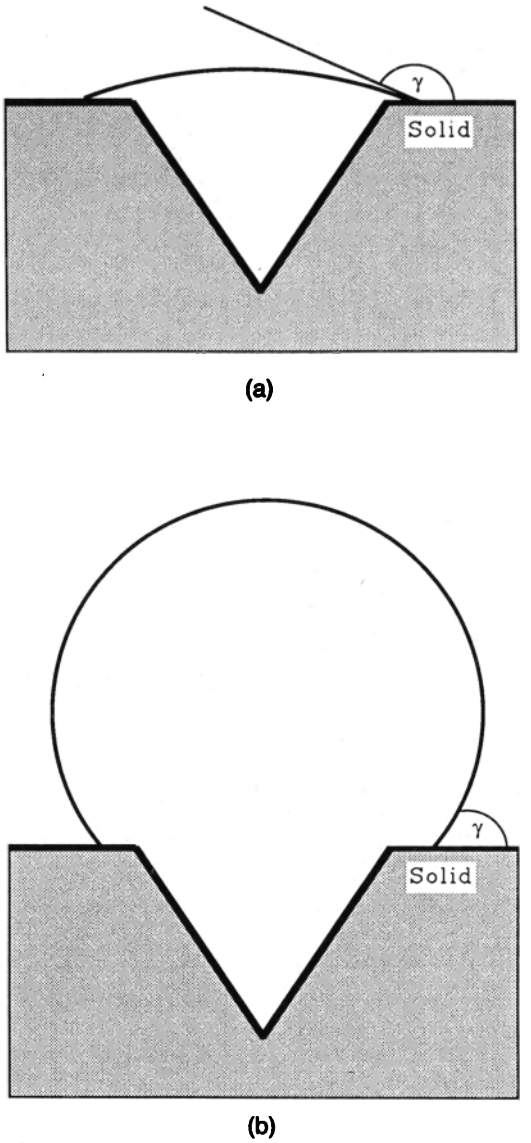

FIG. 7. Diagram showing the two possible configurations for the contact line outside the crevice: (a) $\pi/2 \leqslant \gamma \leqslant \pi$; (b) $0 \leqslant \gamma \leqslant \pi/2$.

$$V = \tfrac{1}{3}\pi a^3(\cot\beta + \eta) = f^+(\alpha,\beta)\,R^3, \tag{13}$$

where

$$\begin{aligned}|\cos^3(\alpha-\beta)|\eta &= [1-\sin(\alpha-\beta)]^2[2+\sin(\alpha-\beta)] \\ &= 2 - 3\sin(\alpha-\beta) + \sin^3(\alpha-\beta) \\ &= 2 - [2+\cos^2(\alpha-\beta)]\sin(\alpha-\beta),\end{aligned} \tag{14}$$

and

$$f^+(\alpha,\beta) = \tfrac{1}{3}\pi(\cot\beta + \eta)|\cos(\alpha-\beta)|^3. \tag{15}$$

When the interface is convex towards the apex [Fig. 6(c)], we have

$$V = \tfrac{1}{3}\pi a^3(\cot\beta - \eta) = f^-(\alpha,\beta)\,R^3, \tag{16}$$

with the same definition of η, and f^- given by (15) with η preceded by a minus sign.

We shall also consider the interface outside the crevice (Fig. 7). In this case the radius of curvature is given by

$$a = R\sin\gamma, \tag{17}$$

if a denotes, as before, the radius of the ring of contact and γ the contact angle with the plane. This relation is valid both for $\pi/2 < \gamma$ [Fig. 7(a)] and for $\gamma < \pi/2$ [Fig. 7(b)]. The volume occupied by the gas is now

$$V = \tfrac{1}{3}\pi a_m^3\cot\beta + \tfrac{1}{3}\pi R^3[2 + (2+\sin^2\gamma)\cos\gamma], \tag{18}$$

again valid in both cases.

Finally, we shall have to refer to these formulas when α equals the receding contact angle α_R or the advancing contact angle α_A. In these cases we shall simply append indices R or A to V, η, or f as appropriate.

V. ANALYSIS OF THE "STANDARD" CREVICE MODEL

As was mentioned earlier, past analyses of the crevice model have only been concerned with the motion of the line of contact [CC' in Fig. 6(a)], without distinction between the stable and unstable cases. A receding contact angle was also assumed such that

$$\beta < \alpha_R < \beta + \pi/2, \tag{19}$$

so that the interface takes the shape of a spherical segment subtending a solid angle less than 2π [Fig. 6(a)]. Although Apfel[20] does include the case $\alpha_R \leqslant \beta$ in his work, he does so in what appears to be an incorrect way as will be noted in Sec. VII. Furthermore, with the exception of a passing comment by Apfel, the fate of the interface as it moves out of the mouth of the crevice has never been addressed. For the lack of better terminology, we refer to the crevice model subject to the limitations (19) as to the "standard" crevice model, and we shall study it in this section in the light of the considerations set forward in Sec. II. In the following sections we shall extend the analysis to features and parameter ranges not previously considered in the literature.

In all of the following we assume that, as the liquid pressure falls, dynamic effects are unimportant and isothermal behavior holds. These assumptions are motivated by the relative rapidity of thermal diffusion and the very high natural frequency of a small gas volume. As already stated, we shall also assume that gas diffusion plays a negligible role so that the gas content of the nucleus remains constant. Therefore, if the index 0 denotes initial conditions, the prefect gas relation $p_G V = p_{G0} V_0$ remains valid throughout the nucleation process to be considered. Since initially the gas pressure in the nucleus p_{G0} equals the gas tension G in the liquid, we have

$$p_G V = V_0 G, \tag{20}$$

with V_0 given by (16):

$$V_0 = \tfrac{1}{3}\pi a_0^3 (\cot\beta - \eta_0). \tag{21}$$

Upon setting $C = -2/R_0$, the equilibrium equation (4) gives, for the initial state,

$$R_0 = 2\sigma/(p_{L0} - p_v - G),$$

or, using (11),

$$a_0 = [2\sigma/(p_{L0} - p_v - G)]\,|\cos(\alpha_0 - \beta)|. \tag{22}$$

In the initial condition the contact angle α is less than, or at most equal to, the advancing contact angle α_A. The actual value of α_0 depends on the gas tension G through (22), which we may rewrite as

$$|\cos(\alpha_0 - \beta)| = (p_{L0} - p_v - G)(a_0/2\sigma). \tag{23}$$

As was mentioned at the end of Sec. I, a gas tension G_A can be defined such that $\alpha = \alpha_A$ when $G = G_A$, while $\alpha < \alpha_A$ when $G > G_A$. By use of (23), G_A is given by

$$G_A = p_{L0} - p_v - (2\sigma/a_0)\,|\cos(\alpha_A - \beta)|. \tag{24}$$

It is clear from this definition that the value of G_A depends on the properties of the nucleus. Conceivably, in a "sufficiently" degassed liquid (in relation to the prevailing distribution of nuclei), $\alpha = \alpha_A$ and $G = G_A$ for most nuclei. This assumption has usually been made in the previous analyses of the standard model.

A. Motion of the interface

Consider an initial state in which the liquid is undersaturated so that the interface is convex towards the gas [Fig. 6(c)]. As the liquid pressure falls, the curvature decreases while the contact line maintains its position. By use of Eqs. (4), (16), and (20), it is easy to write down the equilibrium condition for the interface, namely,

$$p_v + \frac{\cot\beta - \eta_0}{\cot\beta - \eta} G = p_L - \frac{2\sigma}{a_0}|\cos(\alpha - \beta)|. \tag{25}$$

As for the free bubble, Eq. (7), and for the other cases to be discussed below, we have grouped on the left-hand side the terms which tend to promote the growth of the bubble and on the right-hand side those which tend to collapse the cavity. The two sides of this equation are shown qualitatively by the thick (left-hand side) and light (right-hand side) lines in Fig. 8 as a function of α for three values of p_L. In drawing these curves we have used the fact that, for $\alpha > \beta + \pi/2$, η is an increasing function of α and vanishes when the interface is plane, i.e., $\alpha = \beta + \pi/2$. Line a corresponds to the initial state. The two curves intersect at the initial value of the contact angle α_0. As the liquid pressure is decreased (line b), the intersection shifts to the left and the equilibrium value of the contact angle α decreases. It is clear (and it is proven in the Appendix) that only one root exists, provided that

$$p_L > \tilde{\tilde{p}}_L = p_v + (1 - \eta_0 \tan\beta)\, G, \tag{26}$$

i.e., that the interface is convex towards the gas. The expression in the right-hand side of this equation is obtained by setting $\alpha = \beta + \pi/2$ in Eq. (25) and corresponds to line c in Fig. 8. The very existence of a nucleus of the type considered here presupposes that (26) is satisfied in the initial state. For this configuration an increase in the volume of the nucleus corresponds to a decrease of α. The same argument used for the case of the free bubble shows therefore that the equilibrium described by (25) is stable.

When $p_L = \tilde{\tilde{p}}_L$ the interface is plane and a further decrease of the liquid pressure causes it to become concave towards the gas. The sign of the curvature is reversed, and

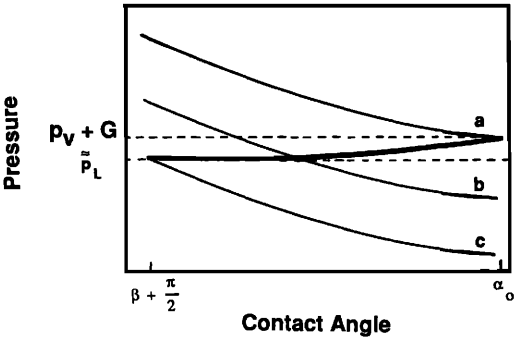

FIG. 8. Graph of the left-hand side (thick line) and the right-hand side (thin lines) of Eq. (25) versus contact angle for three values of p_L: line a—$p_L = p_v + G$, the initial state; line b—$\tilde{\tilde{p}}_L \leqslant p_L \leqslant p_v + G$; line c—$p_L = \tilde{\tilde{p}}_L$. There is only one equilibrium value of α, and it corresponds to a state of stable equilibrium.

the appropriate form of the equilibrium equation is, for $p_L < \tilde{\tilde{p}}_L$,

$$p_v + \frac{\cot\beta - \eta_0}{\cot\beta + \eta} G = p_L + \frac{2\sigma}{a_0}|\cos(\alpha - \beta)|. \quad (27)$$

The two sides of (27) are plotted in Fig. 9 as functions α. When $p_L = \tilde{\tilde{p}}_L$ (line a), the two curves intersect at $\alpha = \beta + \pi/2$ and the interface is flat. As p_L is decreased (line b), the equilibrium value of α shifts to the left, finally reaching α_R (line c). At this point Eq. (27) ceases to apply and the gas–solid–liquid contact line becomes free to move. In this range again there is only one solution which is readily seen to be stable (see Appendix).

When $\alpha = \alpha_R$ the radius of curvature takes on the value

$$R_R = a_0/|\cos(\alpha_R - \beta)|, \quad (28)$$

which may be called the *receding radius*. The corresponding value of the pressure is

$$p_L^A = p_v - \frac{2\sigma}{a_0}|\cos(\alpha_R - \beta)| + \frac{\cot\beta - \eta_0}{\cot\beta + \eta_R} G. \quad (29)$$

At this point the interface is free to move and the appropriate form of the stability equation becomes

$$p_v + K/R^3 = p_L + 2\sigma/R, \quad (30)$$

where, by (13),

$$K = \frac{GV_0}{f^+(\alpha_R,\beta)} = \frac{\cot\beta - \eta_0}{(\cot\beta + \eta_R)|\cos(\alpha_R - \beta)|^3} a_0^3 G.$$

The situation is now very similar to that of a free bubble, and a critical radius exists given by

$$R_c = \left(\frac{3K}{2\sigma}\right)^{1/2} = \frac{4}{3}\frac{\sigma}{p_v - p_L^B}. \quad (31)$$

Solving this equation for p_L^B, the liquid pressure corresponding to R_c, we find

$$p_L^B = p_v - \frac{4}{3}\frac{\sigma}{a_0}\left(\frac{2\sigma}{3a_0 G}\frac{(\cot\beta + \eta_R)|\cos(\alpha_R - \beta)|^3}{\cot\beta - \eta_0}\right)^{1/2}. \quad (32)$$

Two possibilities now exist. If R_R is less than the critical value R_c, the equilibrium is stable and the interface recedes from the bottom of the crevice following the continuing decrease of p_L below p_L^A. In this case, if the decline of p_L were arrested, the interface motion would stop and no bubble would appear. An unstable growth would occur only in a crevice sufficiently deep that as p_L decreases further the radius of the receding interface could reach the value R_c. On the other hand, if $R_R > R_c$, the interface is in unstable equilibrium as soon as the line of contact beocomes free to move. The ensuing growth of the nucleus is triggered by a mechanical instability and would persist even if the decline of the liquid pressure were to stop. It could only be arrested by increasing p_L enough to reestablish one of the conditions described by Eq. (27) or (25). As explained in Sec. II, we believe that only in the case of unstable growth can one speak of a true nucleation event and that therefore the nucleation criterion used by previous investigators,

$$R = R_R, \quad (33)$$

must be replaced by

$$R = \max(R_R, R_c). \quad (34)$$

For the reason mentioned at the end of Sec. II, we call the value of the absolute pressure corresponding to this radius the *first cavitation threshold*. The criterion previously used in connection with the crevice model is correct only when $R_c \leqslant R_R$ or, from (28) and (31),

$$\left(\frac{3V_0 G}{2\sigma f^+(\alpha_R,\beta)}\right)^{1/2} \leqslant \frac{a_0}{|\cos(\alpha_R - \beta)|}, \quad (35)$$

i.e., at sufficiently low gas tensions. The two sides of (35) are equal for $G = G^*$, where

$$G^* = \frac{2\sigma}{3a_0}\frac{(\cot\beta + \eta_R)|\cos(\alpha_R - \beta)|}{\cot\beta - \eta_0}. \quad (36)$$

For $G > G^*$ the critical radius criterion dominates, while for $G < G^*$ the unstable motion begins as soon as $R = R_R$ and the instability threshold coincides with the criterion used by previous investigators. Our results will therefore differ from earlier ones only for $G > G^*$. The quantity $3a_0 G^*/2\sigma$ is plotted as a function of α_R for different values of β in Fig. 10. To give a feeling for the order of magnitude involved, we may note that, for water at 20 °C, $2\sigma/3a_0 = 1$ atm for $a_0 \simeq 0.5\,\mu$m. If the crevice is not deep enough, it is possible for R_R to be

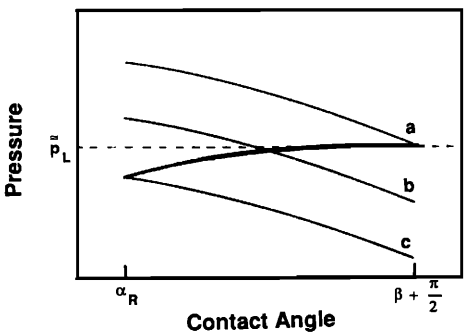

FIG. 9. Graph of the left-hand side (thick line) and the right-hand side (thin lines) of Eq. (27) versus contact angle for three values of p_L: line a—$p_L = \tilde{\tilde{p}}_L$; line b—$\tilde{\tilde{p}}_L \leqslant p_L \leqslant p_L^A$; line c—$p_L = p_L^A$. As in Fig. 8, there is only one equilibrium value of α, and it corresponds to a state of stable equilibrium.

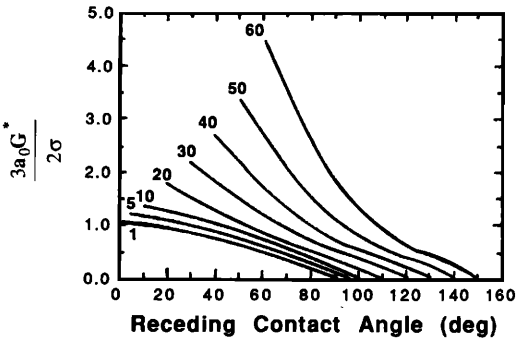

FIG. 10. Graph of the quantity $3a_0 G^*/2\sigma$ [see Eq. (36)] versus the receding contact angle for various values of β from 1° to 60°.

reached, and still be impossible to satisfy $R \geqslant R_c$. It is clear from (28) and (31) that R_R and R_c depend on the geometry and gas content of the crevice, the initial position of the line of contact, and the temperature. In the absence of gas-diffusion effects, these quantities can be considered fixed in a cavitation experiment in which only the liquid pressure p_L varies. In this sense we may consider R_R and R_c as "properties" of each nucleus.

A qualitative insight into how gas diffusion could affect the previous considerations can be obtained in the following way. Suppose that n_0 denotes the number of gas moles in the unperturbed state and $n > n_0$ the number of gas moles during the nucleation process. Then, Eq. (20) must be modified to

$$p_G V = (n/n_0) G V_0,$$

which shows that the "effective" gas concentration during nucleation is greater than in the undisturbed state. The value of G in Eqs. (29) and (32) should therefore be increased. Although this leads to an increase of both thresholds, if n/n_0 is large, the increase of p_L^A is greater than that of p_L^B, and p_L^A will dominate. The earlier condition (33) would then define the appropriate threshold.

B. The first cavitation threshold

We can now connect the parameters corresponding to the initial configuration of the nucleus to the value of the liquid pressure at which the nucleus begins its unstable growth. We call this value the *first* nucleation threshold because, as already mentioned and as will be seen later on, an even lower liquid pressure may be needed to pull the interface out of the crevice, a fact that does not seem to have been appreciated by earlier investigators.

We indicate by the subscript 1 the conditions prevailing at the point where the unstable growth begins. The equilibrium relation (4) is, at this point,

$$p_{G1} = p_{L1} - p_v + (2\sigma/a_1)|\cos(\alpha_R - \beta)|, \tag{37}$$

where again we have used the relation (11) between a and R (recall that now $\alpha = \alpha_R$). Using this relation and Eqs. (13) and (21) in the isothermal law (20), and rearranging, we find

$$p_{L1} = p_v + \frac{\cot\beta - \eta_0}{\cot\beta + \eta_R}\left(\frac{a_0}{a_1}\right)^3 G - \frac{2\sigma}{a_1}|\cos(\alpha_R - \beta)|. \tag{38}$$

Note that $a_1 = a_0$ if the receding radius dominates. However,

$$a_1 = \tfrac{4}{3}[\sigma/(p_v - p_{L1})]|\cos(\alpha_R - \beta)|, \tag{39}$$

if the critical radius dominates. We now treat the two cases separately.

(a) $R_R > R_c$. This is the case in which our results reduce to the earlier ones. Now, $a_0 = a_1$ and (38) reduces to (27), with $\alpha = \alpha_R$:

$$p_v + \frac{\cot\beta - \eta_0}{\cot\beta + \eta_R} G = p_L^A + \frac{2\sigma}{a_0}|\cos(\alpha_R - \beta)|, \tag{40}$$

or, using (22) to eliminate a_0,

$$p_L^A = \left(1 + \frac{\delta_R}{\delta_0}\right)p_v - \frac{\delta_R}{\delta_0}p_{LO} + \left(\frac{\cot\beta - \eta_0}{\cot\beta + \eta_R} + \frac{\delta_R}{\delta_0}\right)G, \tag{41}$$

where we have used the notation

$$\delta = |\cos(\alpha - \beta)|. \tag{42}$$

This relation is valid for $G > G_A$. For $G \leqslant G_A$, $\alpha_0 = \alpha_A$ and Eq. (40) becomes

$$p_L^A = \left(1 + \frac{\delta_R}{\delta_A}\right)p_v - \frac{\delta_R}{\delta_A}p_{LO} + \left(\frac{\cot\beta - \eta_A}{\cot\beta + \eta_R} + \frac{\delta_R}{\delta_A}\right)G. \tag{43}$$

(b) $R_C > R_R$. In this case our results differ from the earlier ones. Now a_1 is given by (39). Upon substitution into (38) and some rearrangement, we find

$$p_L^B = p_v - \frac{4}{3}\sigma\left(\frac{2\sigma\delta_R^3}{a_0^3 G}\frac{\cot\beta + \eta_R}{\cot\beta - \eta_0}\right)^{1/2}, \tag{44}$$

or, using (22),

$$p_L^B = p_v - \frac{2}{3}\left[\left(\frac{\delta_R}{\delta_0}\right)^3\frac{\cot\beta + \eta_R}{\cot\beta - \eta_0}\frac{(p_{LO} - p_v - G)^3}{G}\right]^{1/2}. \tag{45}$$

Again, for sufficiently degassed liquids, $G \leqslant G_A$, $\alpha_0 = \alpha_A$, and

$$p_L^B = p_v - \frac{2}{3}\left[\left(\frac{\delta_R}{\delta_A}\right)^3\frac{\cot\beta + \eta_R}{\cot\beta - \eta_A}\frac{(p_{LO} - p_v - G)^3}{G}\right]^{1/2}. \tag{46}$$

It may be noted that none of these expressions of the threshold equations fully exhibits the dependence on G since δ_0 and η_0 depend on this quantity through (22). It may also be noted that

$$\frac{\cot\beta - \eta_0}{\cot\beta + \eta_R} = \frac{\text{vol. of cone} - \text{vol. of cap with } \alpha = \alpha_0}{\text{vol. of cone} + \text{vol. of cap with } \alpha = \alpha_R}. \tag{47}$$

For limited hysteresis or deep crevices, this ratio will be close to 1, and Eqs. (40) and (44) simplify to

$$p_L^A \simeq p_v + G - A, \tag{48}$$

$$p_L^B \simeq p_v - \tfrac{2}{3}(A^{3/2}/G^{1/2}), \tag{49}$$

where $A = 2\sigma\delta_R/a_0$, while Eqs. (43) and (46), valid for $G \leqslant G_A$, become

$$p_L^A = \left(1 + \frac{\delta_R}{\delta_A}\right)p_v - \frac{\delta_R}{\delta_A}p_{LO} + \left(1 + \frac{\delta_R}{\delta_A}\right)G, \tag{50}$$

$$p_L^B = p_v - \frac{2}{3}\left[\left(\frac{\delta_R}{\delta_A}\right)^3\frac{(p_{LO} - p_v - G)^3}{3G}\right]^{1/2}. \tag{51}$$

With this approximation we therefore see that the results for $G > G_A$ depend on the single parameter A, while those for $G \leqslant G_A$ depend on the single parameter δ_R/δ_A. Equation (50) coincides with Apfel's result, Eq. (13) of Ref. 20.

Since nucleation is, ultimately, a form of boiling, it is intuitively obvious that it can only occur at absolute liquid pressures smaller than p_v. That this is indeed the case when the critical radius criterion dominates is clear from Eqs. (44)–(46). When the receding angle criterion used by pre-

vious investigators dominates, it is easy to show from (40)–(43) that the condition $p_L^A \leqslant p_v$ is satisfied provided that $G \leqslant 3G^*$, with G^* defined by (36). Since, according to the previous considerations, this criterion only dominates for $G < G^*$, this inequality is satisfied. However if, rather than (34), the nucleation criterion is taken to be (33) in all cases as was done by previous investigators, the condition $p_L^A \leqslant p_v$ may fail to be satisfied at high gas concentrations.

As another point we note that, for a saturated liquid for which $G = p_{L0} - p_v$, from the old criterion Eq. (41), we find

$$p_L^A = p_v + \frac{\cot\beta - \eta_0}{\cot\beta + \eta_R}(p_{L0} - \hat{p}_v).$$

In view of the smallness of p_v and the comments made after Eq. (47), it is evident that this value is very close to p_{L0}. In acoustic cavitation, this circumstance reflects in a very small value of the acoustic pressure amplitude. This conclusion is at variance with experiment,[16,25] which unambiguously indicates that the threshold at saturation is not much smaller than, but of the same order as, p_{L0}. We shall return to this point near the end of Sec. VIII.

These weaknesses of the older theory give further indications of its only partial correctness.

VI. INTERFACE BEHAVIOR IN OTHER CASES

One of the limitations of the "standard" model considered in the past is the assumption (19) on the relationship between the receding contact angle α_R and the crevice aperture β. In the present section we shall investigate the motion of the interface in other cases much in the spirit of Sec. V. This analysis is not purely academic since both α_R and β can be expected to vary over a wide range.

A. Wide crevice

We begin by considering the case in which the first inequality of (19) is violated, i.e.,

$$\alpha_R < \beta. \tag{52}$$

This situation may arise in a wide crevice or in the presence of a small receding contact angle. In either case, the interface must exceed a hemisphere before the line of contact can move away from the apex of the crevice [Fig. 6(b)]. As already mentioned, Apfel[20] considers this case but takes as the condition for nucleation that the radius of the spherical cap becomes identical to that of the contact line, so that the interface is a hemisphere. He does not discuss this condition, but it appears to be erroneous since the contact line cannot move until $\alpha = \alpha_R$.

If the liquid is undersaturated, the initial shape of the interface is convex towards the gas as in the previous section and Eq. (25) applies until the liquid pressure has fallen enough that the interface is flat. From this point on, Eq. (27) applies, since the interface is less than hemispherical and convex towards the liquid. As discussed in Sec. V A, both situations are stable. The interface becomes a hemisphere when its radius of curvature equals a_0, and the pressure is

$$p_L = p_v + \frac{\cot\beta - \eta_0}{\cot\beta + 2} G - \frac{2\sigma}{a_0}. \tag{53}$$

A graph of the two sides of Eq. (27) for this value of p_L is given qualitatively by line a in Fig. 11. As p_L is decreased (line b), another root appears with $\alpha < \beta$. It is easy to show that this second root is unstable, while the first one is stable (see the Appendix). As the pressure falls further, the two roots move closer until at some point they coalesce. At still smaller pressures (line c) the expanding forces dominate and no equilibrium is possible. Two possibilities exist. If α_R is reached before the the two roots coalesce, Eq. (27) is no longer applicable from that point on and the existence of the unstable solution is irrelevant. If, on the other hand, the equilibrium turns unstable at a value $\alpha^* > \alpha_R$, a spontaneous expansion from α^* to α_R will take place. Once that α_R has been reached, the rest of the discussion proceeds as for the standard case and the same relations apply.

B. Narrow crevice

We next consider the situation which is established when the second inequality in (19) is violated, i.e., when

$$\beta + \pi/2 < \alpha_R. \tag{54}$$

This situation may occur for a narrow crevice or a very large receding contact angle. In this case the interface remains convex towards the gas as it recedes from the crevice apex [Fig. 6(c)]. As long as $\alpha > \alpha_R$, the contact line does not move, the equilibrium is governed by (25), and is stable. As soon as the value $\alpha = \alpha_R$ is reached, the proper equilibrium equation becomes

$$p_v + K'/R^3 = p_L - 2\sigma/R, \tag{55}$$

where

$$K' = \frac{\cot\beta - \eta_0}{(\cot\beta - \eta_R)|\cos(\alpha_R - \beta)|^3} a_0^3 G.$$

The minimum value of R for this case (corresponding to $\alpha_R = \pi$) is $R = a_0/\cos\beta$, while the maximum is infinite and is attained for $\alpha_R = \beta + \pi/2$. The two sides of (55) are shown in Fig. 12. Equality can occur at most at one point, and this equilibrium position is stable since a slight increase in R would decrease the expanding forces (thick line) and in-

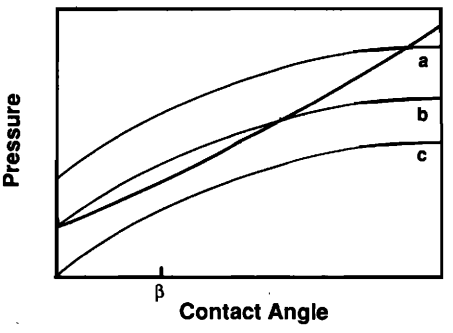

FIG. 11. Graph of the left-hand side (thick line) and the right-hand side (thin lines) of Eq. (27) versus contact angle for three values of p_L: line a—p_L given by Eq. (53); line b—p_L slightly less then the value given by Eq. (53); line c—p_L much less than the value given by Eq. (53). Equation (27) can have one stable solution (line a), one stable and one unstable solution (line b), or no solutions (line c).

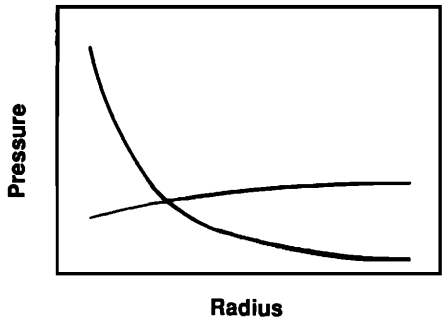

FIG. 12. Graph of the left-hand side (thick line) and the right-hand side (thin line) of Eq. (55) versus radius. The single interaction corresponds to a state of stable equilibrium.

crease the collapsing ones (thin line). Hence, as the pressure falls, the interface starts receding stably as soon as $\alpha = \alpha_R$. The crevice mouth is reached for

$$p_L^m = p_v + \frac{\cot\beta - \eta_0}{\cot\beta - \eta_R}\frac{a_0^3}{a_m^3}G + \frac{2\sigma}{a_m}|\cos(\alpha_R - \beta)|, \tag{56}$$

where a_m is the radius of the mouth. Since all of the terms in the right-hand side of (56) are positive, it may happen that the sum be greater than the initial ambient pressure. This only means that in this case the initial position of the interface is at the crevice's mouth with a value of the contact angle $\alpha_0 > \alpha_R$.

VII. MOTION OUTSIDE THE CREVICE

Another important point never previously discussed in connection with the crevice model is the process by which the interface gets out of the crevice mouth. This is clearly an essential step for the formation of a bubble, and it will be seen in the following that its effect on the nucleation process can be significant.

As for the crevice itself, one needs a geometric model for the crevice mouth, and again as before, there is the risk that the conclusions to be drawn reflect too much of the specific geometrical features of the model and too little of the general aspects of the nucleation process. While we are fully aware of this danger, we do not feel that enough information is available to set up a model free of this problem. Hence, we proceed by postulating the simplest geometrical configuration, that of a conical crevice in an infinite plane surface [Fig. 13(a)]. A simple redefinition of a variable, to be noted below, renders the results obtained in this case also applicable to the situations shown in Fig. 13(b) and (c).

Before we discuss the evolution of the interface when the line of contact reaches the crevice mouth, we note that the following considerations apply only to the case of rapid bubble growth characteristic of flow and acoustic cavitation, and of subcooled boiling. For growth rates so slow that gravity effects are important, as in the case of saturated boiling, a bubble may be pulled by buoyancy out of the crevice mouth.

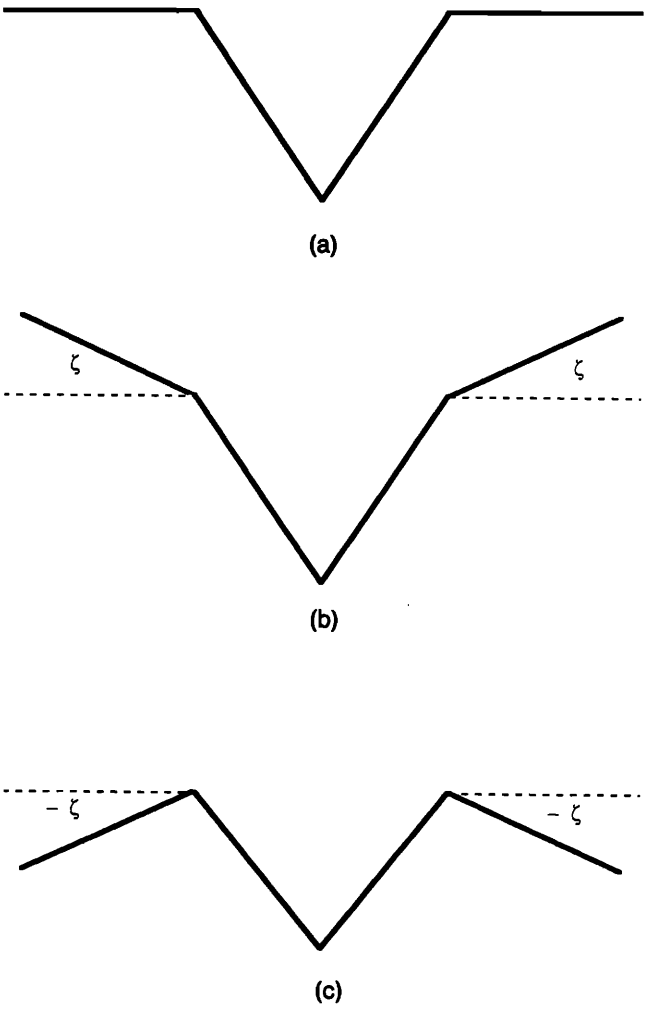

FIG. 13. Diagram showing three possible idealized configurations for the region outside the crevice.

As before, we find two important pressure values, one needed to reach the receding contact angle on the surface outside the crevice and the other one needed to reach conditions of mechanical instability. We call the smaller one of these two (absolute) pressures the *second* cavitation threshold.

The details of the processes to be described are somewhat complicated and are given in full in the Appendix. In this section we shall make use of some approximations.

A. The crevice mouth

The interface starts out at the crevice mouth or reaches it following the dynamics discussed in Secs. V and VI and maintaining an angle α_R with the crevice wall. In the second case, if equilibrium is possible at the mouth, it occurs for a liquid pressure given by

$$p_L^m = p_v + \frac{\cot\beta - \eta_0}{\cot\beta + \eta_R}\frac{a_0^3}{a_m^3}G - \frac{2\sigma}{a_m}|\cos(\alpha_R - \beta)|, \tag{57}$$

whereas in the first case this relation holds with α in place of α_R. This expression holds for "standard" and "wide" crevices. The form applicable to "narrow" crevices has already been given in (56). It can be shown that, depending on the values of the parameters, the value (57) of the liquid pressure can be either larger or smaller than that corresponding to the reaching of the receding radius at the initial position given by (40). In any case, as is shown in the Appendix, (57) is greater than the (aboslute) liquid pressure corresponding to the first nucleation threshold. It can be concluded that (57) does not impose more stringent requirements than those that must already be met for a nucleation event, and is not therefore a particularly significant value of the pressure.

Before the interface can move out of the crevice and onto the plane, the angle γ with the plane (see Fig. 7), which has the value $\alpha_R - \beta + \pi/2$ when the interface first reaches the crevice mouth, must decrease to α_R. During this phase, the equilibrium equation is

$$p_v + \frac{V_0}{V_c}\frac{\sin^3\gamma}{\sin^3\gamma + (a_m^3/V_c)g(\gamma)}G = p_L + \frac{2\sigma}{a_m}\sin\gamma, \tag{58}$$

since the radius of curvature is given by $R = a_m/\sin\gamma$ and the contact line is fixed at the crevice mouth. Here, we have used the definition

$$g(\gamma) = (\pi/3)[2 + (2 + \sin^2\gamma)\cos\gamma], \tag{59}$$

and V_c is the crevice volume given by (12) with $a = a_m$. Let us first simplify (58) by neglecting the gas contribution (last term in the left-hand side). This is a good approximation provided that the initial volume of the gas is small compared with the total volume of the crevice, However, its introduction does not lead to qualitative differences even in other cases. Hence, instead of (58), we consider

$$p_v = p_L + (2\sigma/a_m)\sin\gamma. \tag{60}$$

The two sides of this equation are shown in Fig. 14 for several values of p_L as a function of γ. Note that, in this case, an increase of the nucleus volume corresponds to a decrease of γ. For $p_L > p_v - 2\sigma/a_m$ (line a) the root corresponding to the larger value of γ is stable, while the other one is unstable. For $p_L < p_v - 2\sigma/a_m$ (line c), the expanding forces dominate, the volume tends to increase unstably, and no equilibrium is possible.

Consider now the case of the "standard" model of Sec. V. Here, when the interface gets to the crevice mouth, it is less than a hemisphere, and therefore $\gamma > \pi/2$ and the equilibrium is stable. If $\alpha_R > \pi/2$, the nucleus grows stably as p_L decreases until, for

$$p_L^C = p_v - (2\sigma/a_m)\sin\alpha_R, \tag{61}$$

$\gamma = \alpha_R$ and the contact line is free to move on the plane. If, however, $\alpha_R < \pi/2$, the growth takes place stably only until

$$p_L = p_v - 2\sigma/a_m, \tag{62}$$

(line b in Fig. 14) after which γ passes from $\pi/2$ to α_R in an unstable manner. For the case of a "wide" crevice, on the other hand, the interface starts out with $\gamma < \pi/2$ and grows to $\gamma = \alpha_R$ unstably as soon as it reaches the crevice mouth. In this case this stage of the growth does not introduce any new threshold value for the liquid pressure.

Finally, in the "narrow" crevice case, when the interface reaches the crevice mouth, the appropriate equilibrium equation is (60) with the opposite sign of the surface tension term. It is readily seen that this situation is stable. When $p_L = p_v$ the interface is flat, and as p_L falls below p_v the situation is identical to that of the "standard" case.

Consideration of the gas contribution in the full Eq. (58) has the effect of slightly tilting the thick line counterclockwise. The point of tangency in case (b) is therefore displaced somewhat to the left of $\pi/2$, but the effect is not large for realistic values of the parameters. Taking again this point to be $\pi/2$, we can then replace Eq. (62) by the approximate relation

$$p_L^C \simeq p_v - \frac{2\sigma}{a_m} + \frac{V_0}{V_c}\frac{G}{1 + 2\tan\beta}. \tag{63}$$

It is obvious that the preceding results can be extended to the geometries of Fig. 13(b) and (c) by replacing γ by $\gamma \mp \zeta$, respectively, in the preceding equations.

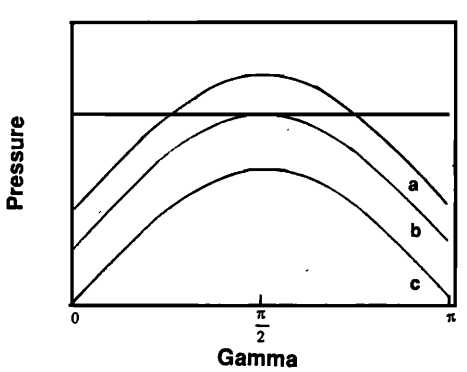

FIG. 14. Graph of the left-hand side (thick line) and the right-hand side (thin lines) of Eq. (60) versus γ for three values of p_L: line a—$p_L > p_v - 2\sigma/a_m$; line b—$p_L = p_v - 2\sigma/a_m$; line c—$p_L \leqslant p_v - 2\sigma/a_m$. Equation (60) can have one stable and one unstable solution (line a) or no solutions (line c). The two solutions merge at $\pi/2$ in line b.

B. Motion outside the crevice

The next and final stage of the nucleation process consists in the motion of the line of contact on the plane away from the crevice mouth. Now, the angle of contact is fixed at the value α_R and the equilibrium equation is

$$p_v + \frac{V_0}{V_c + g(\alpha_R)R^3}G = p_L + \frac{2\sigma}{R}, \tag{64}$$

with the same definition of g previously given in (59). To see what possibilities may arise, we start by considering the case of a deep crevice (or large α_R) for which $V_c \gg g(\alpha_R)R^3$. Then the equation simplifies to

$$p_v + (V_0/V_c)G \simeq p_L + 2\sigma/R. \tag{65}$$

This equation is very similar to that applicable to a pure vapor bubble, and one expects therefore an unstable behavior. Indeed, the lines shown in Fig. 15 indicate that this equilibrium is unstable, so that the unstable growth begins as

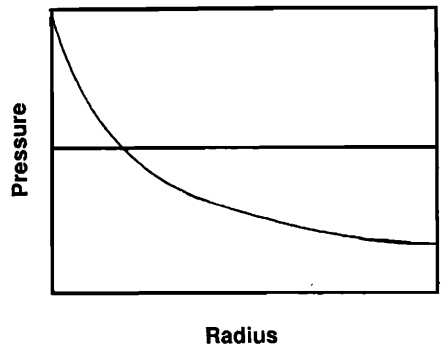

FIG. 15. Graph of the left-hand side (thick line) and the right-hand side (thin line) of Eq. (65) versus radius. The single intersection corresponds to a state of unstable equilibrium.

soon as $\gamma = \alpha_R$ at the crevice mouth. In the opposite case of $V_c \ll R^3 g(\alpha_R)$, Eq. (64) simplifies to

$$p_v + \frac{V_0}{g(\alpha_R)R^3} G = p_L^D + \frac{2\sigma}{R}, \tag{66}$$

which has the same form as for the free bubble. Hence, in this case a critical radius exists given by

$$R_c = \left(\frac{3V_0 G}{2\sigma g(\alpha_R)}\right)^{1/2} = \frac{4}{3}\frac{\sigma}{p_v - p_L^D}. \tag{67}$$

This value can be bigger or smaller than $a_m/\sin\alpha_R$, which is the receding radius for motion on the plane. Equality between the two holds for

$$G^{**} = \frac{2 + (2 + \sin^2\alpha_R)\cos\alpha_R}{(\cot\beta - \eta_0)\sin^2\alpha_R}\left(\frac{a_m}{a_0}\right)^2 \frac{2\sigma}{3a_0}.$$

For $G > G^{**}$, the critical radius exceeds the receding results.

These considerations are sufficient to indicate that the situation described by the complete Eq. (64) is complex. It is shown in the Appendix that it can have one or three real positive roots. In the first case the equilibrium is unstable, while in the second one the middle root is stable and the other two are unstable.

VIII. SOME NUMERICAL RESULTS

The picture that emerges from the previous considerations is unfortunately quite complex. The nucleation process can be dominated by the requirement of unstable growth inside or outside the crevice. In its turn, the threshold thus defined may be determined by the need to reach the receding contact angle or to lose mechanical stability. Depending on the values of the contact angles and of the geometrical parameters, any one of these cases can arise. A given sample of water usually will contain a wide variety of nuclei and general predictions are difficult to make *a priori*. For this reason we have found useful to carry out some numerical studies which will now be illustrated.

According to results obtained in the previous sections, we can identify several "special" values of the liquid pressure p_L of particular importance in the nucleation process, namely the following.

(A) The value p_L^A at which the receding radius is reached in the crevice, given by Eqs. (29) or (40),

$$p_L^A = p_v + \frac{\cot\beta - \eta_0}{\cot\beta \pm \eta_R} G \mp \frac{2\sigma}{a_0} |\cos(\alpha_R - \beta)|. \tag{68}$$

The upper signs apply to the "standard" case (Sec. V), and the lower signs to the "narrow" crevice case (Sec. VI B). For the "wide" crevice case this relation holds with the upper signs if $\alpha_R > \alpha^*$ (Sec. VI A). In the opposite case, α^* should be substituted for α_R, again with the upper signs. Alternative forms are given in Eqs. (41) and (43), and approximate expressions in Eqs. (48) and (50).

(B) The value p_L^B at which the critical radius is reached inside the crevice. This situation never occurs for the "narrow" crevice case, while for the other two, from Eq. (45), it occurs for

$$p_L^B = p_v - \frac{4\sigma}{3a_0}\left(\frac{2\sigma}{3a_0 G}\frac{(\cot\beta + \eta_R)|\cos(\alpha_R - \beta)|^3}{\cot\beta - \eta_0}\right)^{1/2}. \tag{69}$$

Other expressions for this quantity are given in (46), (49), and (51), the last two being approximations. The smaller of p_L^A and p_L^B was indicated earlier as the *first* cavitation threshold.

(C) The value p_L^C at which the interface forms an angle α_R with the plane. This value is unstable for the "wide crevice" case, while common expressions apply in the other two cases. If $\alpha_R > \pi/2$, it is given approximately by

$$p_L^C \simeq p_v - (2\sigma/a_m)\sin\alpha_R, \tag{70}$$

while if $\alpha_R < \pi/2$, it is sufficient to reach

$$p_L^C \simeq p_v - \frac{2\sigma}{a_m} + \frac{\cot\beta - \eta_0}{2 + \cot\beta}\frac{a_0^3}{a_m^3} G, \tag{71}$$

approximately. Exact relations are used in the calculations to be described.

(D) The value of p_L^D necessary to reach the critical radius on the plane. When the crevice volume is smaller than the volume of the spherical segment, Eq. (67) leads to the approximate expression

$$p_L^D \simeq p_v - \frac{4\sigma}{3a_0}\left(\frac{2\sigma}{3a_0 G}\frac{2 + (2 + \sin^2\alpha_R)\cos\alpha_R}{\cot\beta - \eta_0}\right)^{1/2}. \tag{72}$$

In the opposite (and much more frequent) case in which the volume of the crevice is much larger than that of the spherical segment, the interface is already unstable when p_L^C is reached and the value of p_L^D is irrelevant. In the intermediate case in which the two volumes are comparable, the complete Eq. (64) must be used. In the calculations that follow, the exact values obtained from this complete equation have been used. The smaller value between p_L^C and p_L^D was called in the previous section the *second* nucleation threshold.

For a nucleation event to occur, the liquid pressure must fall below the lowest one of these pressure values $p_L^A, \ldots, p_L^D$. Unfortunately, it is not possible to establish an ordering among them valid in all circumstances, and therefore it is not possible to arrive at a unique criterion for nucleation. These considerations motivated the parametric study that will now

be described. A more detailed numerical study will form the object of a separate publication.

The numerical results to be shown are of two different types. The first series of figures is a plot of the volume V_G occupied by the gas versus $p_v - p_L$. We show the evolution of the bubble volume as the liquid pressure falls until the interface is on the plane outside the crevice and the radius of the contact ring equals $3a_m$. The critical pressures $p_L^A,\ldots,p_L^D$ are indicated in the graphs. (For brevity, the symbol p_L^X is used in the figures in place of $p_v - p_L^X$, with $X = A,B,C,D$.) The second set of figures shows the dependence of the pressures p_L^X on G, all other parameters being constant. Though certainly not exhaustive, these examples demonstrate a number of important points.

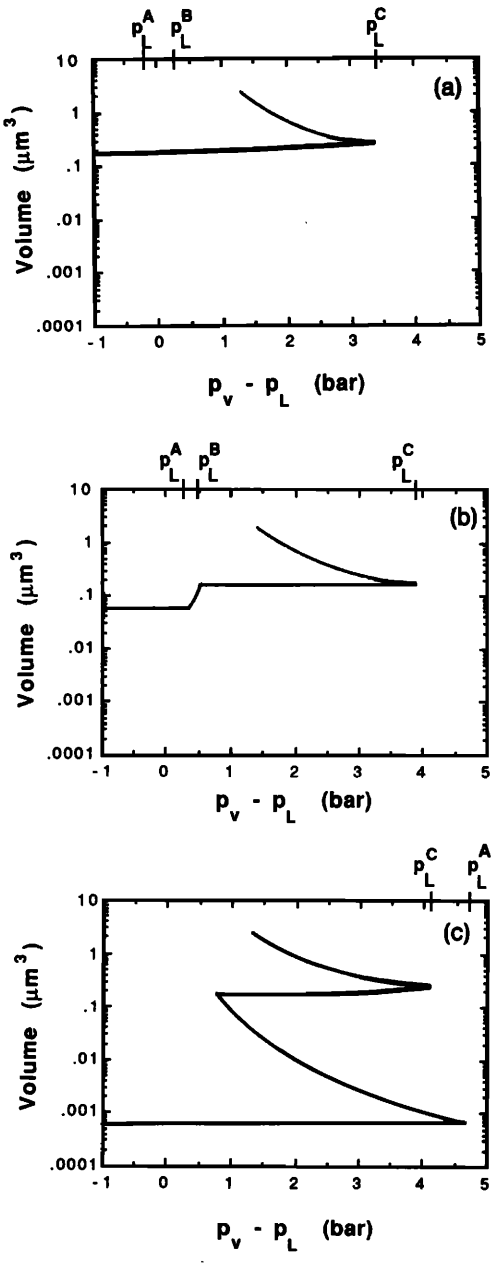

FIG. 16. Graph of the volume of the nucleus versus $p_v - p_L$ for a "standard" crevice case [$\beta \leqslant \alpha_R \leqslant \pi/2 + \beta$; see Fig. 6(a)] and different values of the gas concentration G. In this set of figures, $a_m = 0.35\,\mu$m, $\alpha_A = 106°$, $\alpha_R = 94°$, $\beta = 15°$, $\sigma = 0.072$ N m^{-1}, $p_{L0} = 0.975$ bar, and $p_v = 0.025$ bar. (a) $G = 0.975$ bar, (b) $G = 0.88$ bar and (c) $G = 0.5$ bar. The notation p_L^A, p_L^B, and p_L^C at the top of the graph is shorthand for $p_v - p_L^A$, $p_v - p_L^B$, and $p_v - p_L^C$.

The figures of the first set refer respectively to examples of a "standard" crevice (Fig. 16), a wide crevice (Fig. 17), and a narrow crevice (Fig. 18). In each case we present results for different values of the gas tension G. The largest value is 1 bar and corresponds to saturation since the liquid pressure is taken to equal 1 bar initially ($p_v - p_L \simeq -1$ bar). For this value of G the interface is assumed to be flat and located at the crevice's mouth when the liquid pressure starts to fall so that $a_0 = a_m$. As the gas tension G is decreased, the initial position of the interface is assumed to be at the crevice's mouth and to form a progressively increasing angle α with the crevice wall until the value α_A is reached. For lower values of G, the initial contact angle is taken to remain fixed at α_A, but the initial interface position is assumed to be deeper and deeper into the crevice. In other words, for any value of G, the starting configuration of the interface is taken to be such that the value of G in question coincides with the quantity G_A defined in Eq. (24). The choice of these initial conditions is motivated by the description given in the last paragraph of Sec. I. Ideally, this procedure corresponds to an experiment in which the threshold is measured for progressively decreasing dissolved gas contents. Other procedures are possible. For example, for each value of G, one might assume an initial configuration consistent with a prepressurization of the liquid.

The "standard" crevice example is considered first in Fig. 16. The parameters are given in the figure caption and, with the exception of G, are the same in each case. The case corresponding to saturation is shown in Fig. 16(a) for which $G^* = 0.27$ bar. As the liquid pressure is decreased from 1 bar, the radius of curvature decreases from infinity, the interface bows outward, and reaches the receding contact angle. The value of the pressure at which this happens corresponds to p_L^A given by Eq. (68). [Recall that the pressure value marked as p_L^A in Fig. 16(a) actually indicates $p_v - p_L^A$. The same is true for all such pressures indicated at the top of Figs. 16–18.] According to the previous versions of the crevice model, nucleation would occur at this point. However, before nucleation can occur according to the present theory, three other conditions must be checked, namely, p_L^B, p_L^C, and p_L^D. In this case $p_v - p_L^B$ is greater than $p_v - p_L^A$, indicating that the critical radius has not yet been exceeded, and so the nucleus is not unstable. Strictly speaking, though, p_L^B will never be reached because the interface starts out at the mouth. Hence, the evolution of the nucleus from $\alpha = \alpha_R$ at p_L^A onward involves "rounding" the mouth and, therefore attention must be shifted to p_L^C and p_L^D. During this process, the interface must go from forming an angle α_R with the crevice wall to forming an angle α_R with the plane, continually decreasing R along the way. Hence, the path from p_L^A to p_L^C is a continuous increase in $p_v - p_L$. The contact angle reaches α_R with the plane at p_L^C. From this point on the interface spreads out over the plane away from the crevice.

This spreading out causes an increase in R, a decrease in the Laplace pressure, and so a decrease in $p_v - p_L$ as indicated in Fig. 16(a). In this example, $V_c \gg g(\alpha_R)R^3$. Therefore, Eq. (65) is a good approximation to Eq. (64) and, as shown in Fig. 15, unstable growth begins as soon as $\gamma = \alpha_R$ at p_L^C. In such a case p_L^D is irrelevant. In conclusion, for this example, the threshold for unstable growth is p_L^C. This result is in marked contrast to that of previous versions of the crevice model which would predict the threshold to be p_L^A.

The gas tension G has been reduced to 0.88 bar in Fig. 16(b). This reduction in G causes the interface in the initial configuration to have advanced toward the apex of the crevice and $a_0 = 0.25\ \mu$m so that $a_0/a_m \simeq 0.71$, with $G^* = 0.38$ bar. The initial volume V_0 (at $p_v - p_L \simeq -1$ bar) is therefore smaller. As p_L is decreased, the interface begins to bow outward and the volume increases. At p_L^A, α equals α_R. The difference $p_v - p_L^A$ is larger in this case than in the first one due to the reduction in a_0. Hence, $R\ [= a_0/|\cos(\alpha_R - \beta)|]$ is smaller and the Laplace pressure is larger [see Eq. (29)]. Again, the previous versions of the crevice model would have predicted nucleation at this point, but as can be seen in Fig. 16(b), p_L^B has not been reached and so the nucleus is still in a state of stable equilibrium and nucleation cannot occur. Any further increase in the volume of the nucleus can only take place in response to a reduction in p_L. This increase in volume occurs as the interface recedes away from the crevice apex maintaining α equal to α_R. Eventually, the liquid pressure would equal p_L^B and the nucleus becomes unstable. However, in this example, when p_L^B is reached the interface is at the mouth of the crevice and any further growth involves rounding the mouth. Upon a further decrease in p_L, the interface bows outward until $\gamma = \alpha_R$ at p_L^C. The value of $p_v - p_L^C$ in Fig. 16(b) is larger than that in Fig. 16(a) because the gas partial pressure, and hence the net expanding force, is less in the second case owing to the smaller initial volume. The evolution of the nucleus from p_L^C is the same as in Fig. 16(a). Again, the nucleation threshold is given by p_L^C, in contrast to previous predictions.

Finally, in Fig. 16(c), G has been reduced to 0.5 bar, $a_0 = 0.053\ \mu$m, $a_0/a_m \simeq 0.15$, and $G^* = 1.8$ bars. As in the second case, the interface starts from within the crevice and the evolution is similar. The difference $p_v - p_L^A$ is much larger owing to the much smaller value of a_0. Also, because G is smaller, the receding radius is reached at a pressure p_L^A greater than the pressure $p_L^B \simeq -6.5$ bars at which the motion inside the crevice becomes unstable. At p_L^A, the interface starts receding stably from the apex and reaches the crevice's mouth before p_L has fallen to the level p_L^B. This quantity, therefore, plays no role in this example. The evolution from p_L^A is essentially the same as before, but $p_v - p_L^C$ is less than $p_v - p_L^A$ in this case. Therefore, the cavitation threshold corresponds to p_L^A in agreement with previous versions of the crevice model.

An example of a wide crevice case, for which $\alpha_R < \beta$, is shown in Fig. 17. The gas tension G is equal to 1 bar in Fig. 17(a) and the interface starts from the mouth as in Fig. 16(a). Here $G^* = 2.29$ bars. As p_L is decreased, the interface bows outward and R decreases. Again, as in the previous example, $V_c \gg g(\alpha_R)R^3$ and therefore Eq. (65) is a good approximation to Eq. (64). Unstable growth begins as soon as $\gamma = \alpha_R$ at $p_v - p_L^C = 0.43$ bar. [For this case, the surface would be hemispherical for $p_v - p_L = 3.46$ bars and the value p_L^A would be reached for $p_v - p_L^A = 3.47$ bars.]

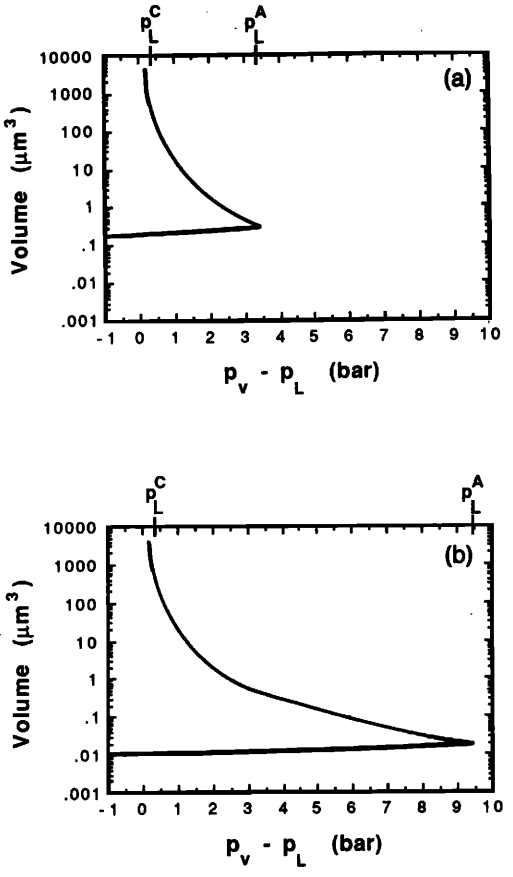

FIG. 17. Graph of the volume of the nucleus versus $p_v - p_L$ for a wide crevice case [$0 \leqslant \alpha_R \leqslant \beta$; see Fig. 6(b)] and different values of the gas concentration G. In this set of figures, $a_m = 0.35\ \mu$m, $\alpha_A = 106°$, $\alpha_R = 6°$, $\beta = 15°$, $\sigma = 0.072$ N m^{-1}, $p_{L0} = 0.975$ bar, and $p_v = 0.025$ bar. (a) $G = 0.975$ bar and (b) $G = 0.8$ bar. The notation p_L^A and p_L^C at the top of the graph is shorthand for $p_v - p_L^A$ and $p_v - p_L^C$.

In Fig. 17(b), G has been reduced to 0.8 bar and the interface starts from within the crevice with $a_0 = 0.14\ \mu$m, $a_0/a_m = 0.41$, and $G^* = 5.58$ bars. The interface becomes hemispherical at $p_v - p_L = 9.51$ bars and $p_v - p_L^A = 9.43$ bars. Therefore, in contrast to the first case, the nucleus becomes unstable somewhere along the evolution between $\alpha = \beta$ and $\alpha = \alpha_R$. Once at $\alpha = \alpha_R$, the nucleus is still unstable and growth continues. In this case the threshold for unstable growth is essentially, but not exactly, equal to p_L^A. Though not in this example, there may be some set of parameters for which the difference in the true threshold and p_L^A is significant.

Finally, a narrow crevice example, for which $\pi/2 + \beta \leqslant \alpha_R \leqslant \alpha_A$, is considered in Fig. 18. In Fig. 18(a), $G = 1$ bar. The reader will notice that the value of p_L^A is not indicated in the graph. The reason is that in a narrow crevice,

with this value of G, the interface must be bowed inward in order for α to equal α_R. Therefore, it would be necessary to overpressurize the liquid ($p_v - p_L < -1$ bar) in order to force the interface to start at α_R. The entire evolution for the case shown in Fig. 18(a) consists of rounding the mouth. The lowest liquid pressure occurs at p_L^C and evolution beyond that point is unstable.

In Fig. 18(b), $G = 0.5$ bar, $a_0 = 0.35$ μm, and $a_0/a_m = 1$. In this case, the interface starts at a contact angle greater than α_R and therefore p_L^A is meaningful. However, the reduction in G is not sufficient to cause the interface to reach α_A and so the initital position is at the mouth of the crevice as in the previous case. The evolution is essentially the same as in Fig. 18(a). It should be further recalled that p_L^B is not defined for narrow crevices.

In Fig. 18(c), G has been reduced to 0.1 bar, which is sufficient to cause the interface to start from a position inside the crevice. In this case, $a_0 = 0.31$ μm, and $a_0/a_m = 0.90$. When p_L is reduced to p_L^A, $\alpha = \alpha_R$ and the interface starts to recede stably to the crevice mouth. This leads to a nearly stepwise behavior of the curve because the rate of volume increase when the interface is free to move is much greater than when the contact line is fixed and only the radius of curvature can change. From this point on the evolution consists of rounding the mouth and spreading out over the plane and follows the now familiar pattern.

Conspicuously absent from these examples is a case where the threshold for unstable growth is governed by p_L^D, which is the value necessary to reach the critical radius on the plane. There are two reasons for this. First, the concept of p_L^D is meaningful only when Eq. (64) has three real roots, because in the opposite case the equilibrium is unstable as soon as the receding angle α_R is reached. Three real roots occur when $V_c < g(\alpha_R)R^3$, a condition which in the previous examples is only verified for the case of Fig. 17 (due to the extremely small value of α_R) and which may indeed be rare in nature. Second, when Eq. (64) does have three real roots, p_L^D dominates only provided that $G > G^{**}$ defined in (67). For the cases of Fig. 17(a) and (b), we find such large values of G^{**} (equal to 135 and 1951 bars, respectively) that this condition is evidently not met. We have verified numerically the dominance of p_L^D for cases in which $G > G^{**}$, but we do not present any such example here. For completeness we give the values of G^{**} for the examples of Figs. 16 and 18, although, for the reasons just stated, they are not needed to reach the conclusions presented above. For Fig. 16(a), (b), and (c), $G^{**} = 0.66$, 1.79, and 1.92 bars, respectively, while for Fig. 18(a), (b), and (c), $G^{**} = 0.45$, 0.46, and 0.65 bar.

The dependence of the cavitation thresholds on gas tension is shown in Fig. 19 for the three cases presented here. The quantities plotted are $p_v - p_L^A$, $p_v - p_L^B$, and $p_v - p_L^C$. The last threshold, $p_v - p_L^D$, is of no interest for these examples, as explained before. Figure 19(a) refers to the case of Fig. 16, namely, a standard crevice. The pressure p_L^B necessary to reach the critical radius in the crevice dominates only for G greater than G^*, which here is approximately 0.77 bar. For this value the two curves p_L^A and p_L^B are tangent. Since in this example the curve labeled p_L^C lies above the others for G greater than about 0.55 bar, it is concluded that p_L^B plays no role. Hence, the receding radius criterion inside the crevice, $p_v - p_L^A$, dominates for G less than 0.55 bar, while at greater saturations the receding radius criterion outside the crevice, $p_v - p_L^C$, dominates. The previous versions of the crevice model are consistent with the first result (i.e., at low gas concentration), but not with the second one. It is interesting

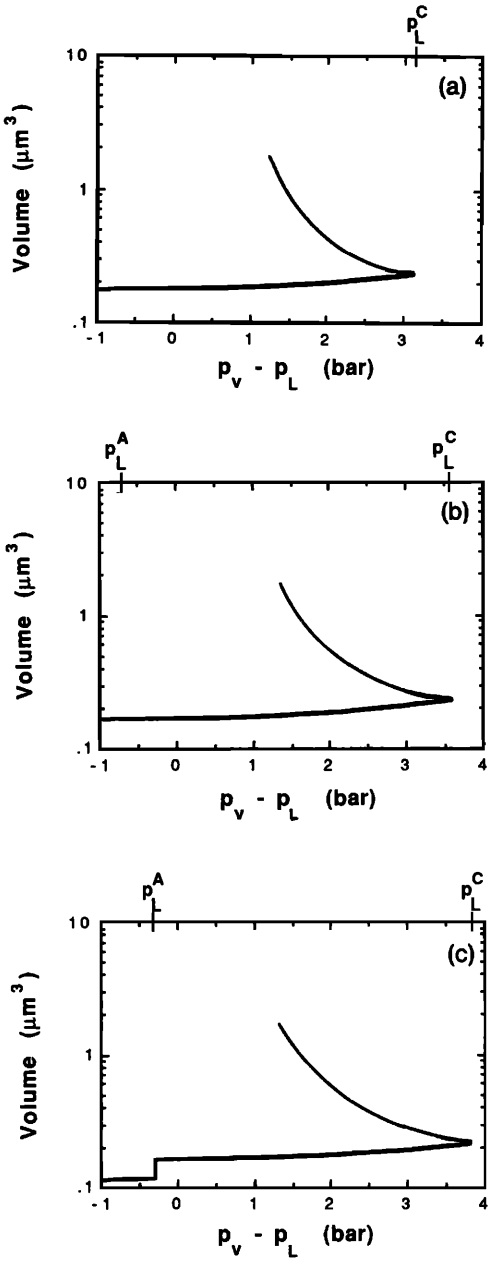

FIG. 18. Graph of the volume of the nucleus versus $p_v - p_L$ for a narrow crevice case [$\pi/2 + \beta \leqslant \alpha_R \leqslant \alpha_A$; see Fig. 6(c)] and different values of the gas concentration G. In this set of figures, $a_m = 0.35$ μm, $\alpha_A = 116°$, $\alpha_R = 108°$, $\beta = 15°$, $\sigma = 0.072$ N m^{-1}, $p_{L0} = 0.975$ bar, and $p_v = 0.025$ bar. (a) $G = 0.975$ bar, (b) $G = 0.5$ bar, and (c) $G = 0.1$ bar. The notation p_L^A and p_L^C at the top of the graph is shorthand for $p_v - p_L^A$ and $p_v - p_L^C$.

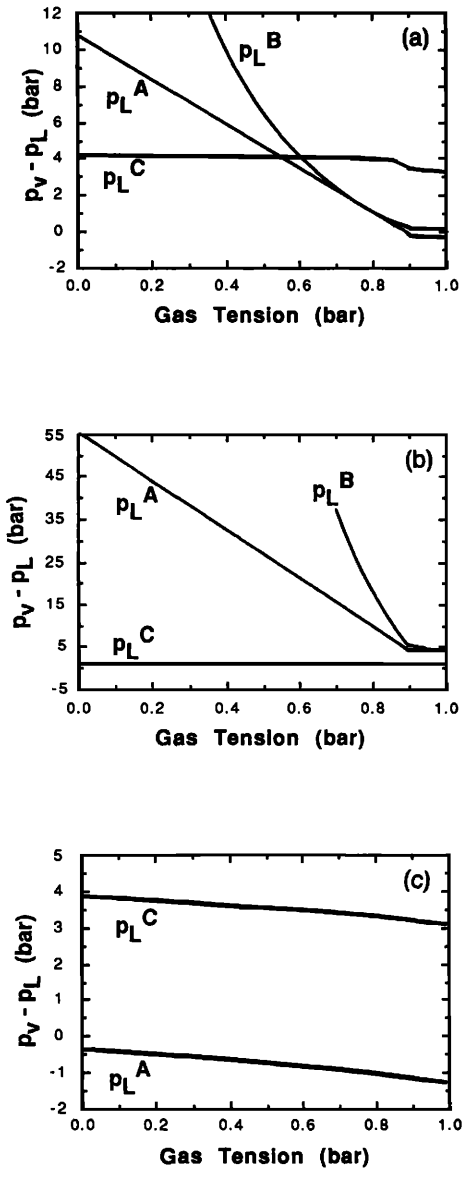

FIG. 19. Thresholds versus gas concentration for the examples of the previous three figures. (a) refers to the case of Fig. 16, (b) to that of Fig. 17, and (c) to that of Fig. 18.

to note that, whereas $p_v - p_L^A$ goes to a value close to -1 bar at $G = 1$ bar (see the end of Sec. V), $p_v - p_L^C$ approaches approximately 3.5 bars. Thus the older version of the crevice model predicts an acoustic pressure amplitude close to 0 as the threshold for a cavitation in a saturated liquid at 1 bar, while the present model gives a nonzero value equal, for the parameters of this example, to 4.5 bars. As already mentioned, experiments show beyond doubt that the acoustic threshold is not zero in saturated liquids.[16,25] Therefore, the present model matches experimental results better than previous versions of the crevice model. A more detailed comparison of the predictions of this model with experimental results will be the topic of a future paper.

Figure 19(b) refers to the wide crevice example shown in Fig. 17. In this case $G < G^*$ in the entire range. Again, therefore, although the line $p_v - p_L^B$ appears to lie above $p_v - p_L^A$, this threshold value plays no role and p_L^A dominates for all values of G. The change in slope at $G \simeq 0.9$ bar is the result of the fact that, for lower values of G, the interface reaches the advancing contact angle and moves toward the apex as G is decreased, while for greater values of G the interface remains at the crevice mouth.

Finally, the narrow crevice example of Fig. 18 is considered in Fig. 19(c). It is seen in the figure that $p_v - p_L^A$ is negative, so that the pressure required to reach the receding contact angle is positive, or, at any rate, greater than p_v. This feature is readily explainable in terms of the peculiarities of this case. Here, it is seen that p_L^C dominates over the entire range of concentrations shown.

IX. CONCLUSIONS

In this paper we have developed the crevice model of nucleation in two directions. In the first place (Sec. II) we have argued that a true nucleation event must be the result of the loss of mechanical stability of the nucleus. Second, we have considered the question of the motion of the interface outside the crevice and investigated parameter ranges different from those considered thus far in the literature. Our analysis has shown the crevice model to exhibit a much richer behavior than previously realized. While this can account for the variability of the cavitation threshold measured on the same liquid sample, it is also true that this variability is usually limited.[16] This feature may be either a consequence of the fact that the nuclei present in a given sample are fairly similar, or of the relative insensitivity of the threshold to the parameter values in some regions of the parameter space. Some indications that this may be the case were obtained by the limited numerical study of Sec. VIII. However, more data, both experimental and numerical, will be needed to reach firmer conclusions.

Our results seem to indicate that the nucleation thresholds calculated from the earlier versions of the crevice model coincide with ours only at low gas concentrations. At larger gas concentrations our results lead to more stringent nucleation criteria, i.e., more negative absolute pressures. This feature appears consistent with the available data.

When the nucleus is first wetted, whether gas is trapped in the crevice or not may have an important effect on the final positon of the liquid surface and, through this, on its ultimate strength. Other than this mechanism, which is not considered in the present study, it is intuitively clear that, for a given initial configuration, the effect of the gas can at most introduce a difference with the pure-vapor thresholds, given by conditions (68) or (71) with $G = 0$, of the order of G. Therefore, the results of our analysis would be quantitatively significant only in cases in which the threshold is at most a few times G, rather than many times G. For $G \sim 1$ bar, this would be the case for nuclei greater than, say, 0.1 μm. On the other hand, for large nuclei (bigger than, say, a few micrometers), the threshold is not much different from p_v and our results introduce but a small correction to this value. Hence, the mechanisms described above are of significance only in the range between tenths of micrometers and a few microme-

ters, which is the crucial decade for nucleation in water in normal conditions.

An interesting experiment which might be carried out to further explore the nucleation process consists in the generation of cavitation events one at a time by the use of very small water samples. In this way spectra of the nuclei distribution in different water samples could be generated. Another useful approach appears to be the simultaneous use of different techniques of bubble generation on different samples drawn from the same water batch. Side by side with acoustic and flow cavitation, boiling could be employed. For high-frequency acoustic cavitation, gas-diffusion effects are unimportant and the present theory should apply. At lower frequencies or in flow cavitation, gas diffusion should be important and a different nucleation behavior would be expected. Finally, in boiling, permanent gas must have a negligible effect and a still different behavior should be observed.

ACKNOWLEDGMENTS

The authors wish to express their gratitude to Professor Robert E. Apfel and to the reviewers for a number of very useful suggestions. The initial portion of this study has been supported by the Office of Naval Research. Subsequent work has been supported by the F. V. Hunt Postdoctoral Fellowship and NPS Research Foundation for the first author, and by the National Science Foundation for the second author.

APPENDIX

The conclusions reached in this paper depend upon the number of roots of each equilibrium equation and their stability. Here, we give some details on the manner by which the results stated in the main text have been obtained.

1. Equation (25)

In terms of $\delta = |\cos(\alpha - \beta)|$, we have from (14), for $\alpha > \beta$,

$$\eta = \delta^{-3}[2 - (2+\delta^2)(1-\delta^2)^{1/2}], \qquad \frac{d\eta}{d\delta} = 3\,\frac{2 - \delta^2 - 2(1-\delta^2)^{1/2}}{\delta^4(1-\delta^2)^{1/2}}. \tag{A1}$$

Hence, η, as a function of δ, is monotonically increasing from $\eta(0) = 0$ to $\eta(1) = 2$. In the range of present concern, $\alpha > \beta + \pi/2$ so that, as the volume increases and α decreases, η also decreases. The left-hand side of (25), therefore, decreases with decreasing α from the value $p_v + G$ it has initially. The right-hand side, on the other hand, equals p_L for $\alpha = \beta + \pi/2$, and decreases as α increases. Hence, the two lines, if they cross (as they must for the situation envisaged to exist), can only cross once at a *stable* point (Fig. 8). This point moves towards the direction of decreasing α as p_L decreases, so that the interface tends to become more flat.

2. Equation (27), "standard" case

Now, the range is $\beta < \alpha_R \leqslant \alpha \leqslant \beta + \pi/2$ so that η decreases as α increases. Since, however, η appears with the opposite sign in (27) as compared with (25), we again conclude that the left-hand side of (27) is an increasing function of α, while the right-hand side is a decreasing function of α. The situation is therefore qualitatively the same as before (Fig. 9).

3. Equation (27), "wide crevice" case

The range is now $0 \leqslant \alpha_R \leqslant \alpha \leqslant \beta$. Let

$$P = \frac{p_v - p_L}{2\sigma/a_0}, \quad A = \frac{V_0 G}{(2\sigma/a_0)(\pi/3)a_0^3},$$

and rewrite Eq. (27) in the form

$$P + \frac{A\delta^3}{\delta^3 \cot\beta + 2 + (2+\delta^2)(1-\delta^2)^{1/2}} = \delta, \tag{A2}$$

where $\delta = \cos(\alpha - \beta)$. The derivative of the left-hand side is

$$\frac{d}{d\delta}[\text{lhs of (A2)}] = 3A\delta^2\,\frac{2(1-\delta^2)^{1/2} + 2 - \delta^2}{(1-\delta^2)^{1/2}[\delta^3 \cot\beta + 2 + (2+\delta^2)(1-\delta^2)^{1/2}]^2},$$

is always non-negative, and vanishes for $\delta = 0$, while it tends to infinity as $\delta \to 1$. This case starts to exist when the interface becomes hemispherical, i.e., $\alpha = \beta$, and therefore, from (A2), $\delta = 1$ and $P = \overline{P}$ with

$$\overline{P} + A/(2 + \cot\beta) = 1,$$

which is the same as (53). The two sides of (A2) are plotted for this value of P in Fig. A1 where, in addition to the intersection for $\delta = 1$, another root is seen to exist (Fig. A1, line a).

To examine the stability of these solutions we note that, for the present case, an increase of the volume corresponds to a decrease of α below β, and therefore to a decrease of δ below 1. The curves in Fig. A1 show that, for such a decrease of δ, the right-hand side of (A2), which arises from surface tension, dominates. We therefore conclude that the equilibrium at $\delta = 1$ is stable, while the same argument proves the other root (which is, however, irrelevant for the present) to be unstable.

As the liquid pressure falls further, P increases (recall that $p_L < 0$), and the curve representing the left-hand side of (A2) translates upward as shown in Fig. A1, line b.

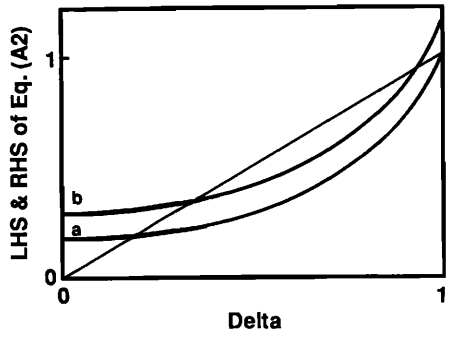

FIG. A1. Graph of the left-hand side (thick lines) and the right-side hand side (thin line) of Eq. (A2) versus δ for two values of P: line a—$P = 1 - A/(2 + \cot\beta)$ and line b—$P < 1 = A/(2 + \cot\beta)$.

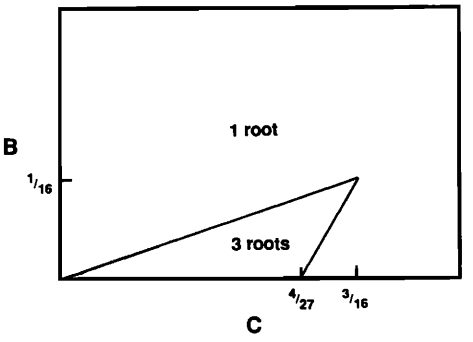

FIG. A3. Regions of the (C,B) plane where Eq (64), or (A4), has one or three equilibrium solutions. On the lines two roots coalesce and the equation has only two distinct solutions.

4. Equation (64)

Let

$$x = [(p_v - p_L)/2\sigma]R,$$

$$B = \frac{(p_v - p_L)^3 V_c}{8\sigma^3 g(\alpha_R)}, \quad C = \frac{(p_v - p_L)^2 V_0 G}{8\sigma^3 g(\alpha_R)}.$$

Then, Eq. (64) becomes

$$1 + C/(B + x^3) = 1/x, \tag{A3}$$

or

$$x^4 - x^3 + (B + C)x - B = 0. \tag{A4}$$

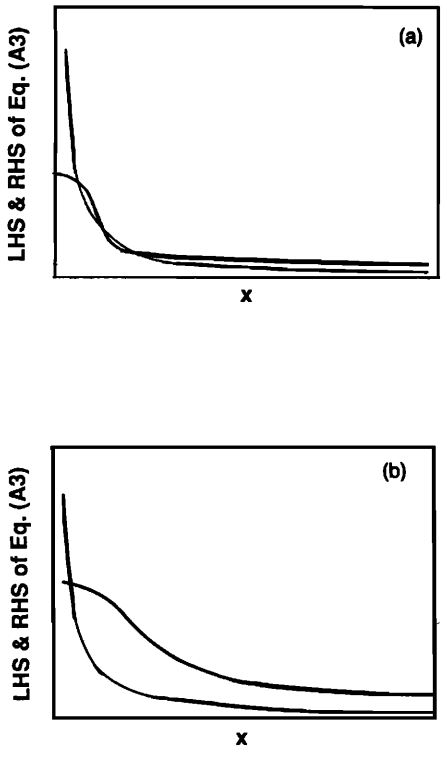

FIG. A2. Graph of the left-hand side (thick line) and the right-hand side (thin line) of Eq. (A3) versus x showing that there can be either (a) three roots or (b) one root.

The two sides of (A3) are plotted qualitatively in Fig. A2. It is evident (and can also be proven otherwise) that at most three acceptable roots exist. If there is only one root, the usual argument proves it to be unstable. If there are three roots, the middle one is stable and the other two are unstable. To find the condition for which all these roots coincide, we note that, in this case, Eq. (A4) must have the form $(x - r)^3(x + s)$. Expanding and comparing with (A4), we find $r = s$ and $r = 1/2$, $B = 1/16$, and $C = 3/16$. To find the condition for which two roots coincide, we compare (A4) with $(x^2 + px + q)(x - r)^2$. This leads to $p = 2r - 1$, $q = r(2p - r)$, and

$$B = r^3(2 - 3r), \quad C = 3r^2(1 - r)^2.$$

These relations can be considered as the parametric form of the two-root lines in the (B,C) plane (Fig. A3). The range $0 \leqslant r \leqslant 1/2$ gives the upper line where the two smaller roots coincide; the range $1/2 \leqslant r \leqslant 2/3$ gives the lower boundary where the two larger roots coincide. The point where the two lines meet corresponds to the three coincident roots found before. Inside the triangular region there are three distinct roots [Fig. A2(b)], while outside only one root exists [Fig. A2(a)]. The approximation $V_c \gg g(\alpha_R)R^3$ used in the main text corresponds to approximating (A4) by

$$(B + C)x - B = 0,$$

while the opposite approximation leads to

$$x(x^3 - x^2 + C) = 0.$$

In the first case B is large and in the second one small.

5. Pressure to reach the crevice mouth

Some statements have been made in Sec. VII after Eq. (57) concerning the ordering of the absolute liquid pressure p_L^m necessary for the interface to reach the crevice's mouth in the "standard" and "wide" crevice cases, and p_L^A and p_L^B. We now give proofs of these statements.

In terms of the quantity G^* defined in (36), Eq. (68) for p_L^A may be written

$$p_L^A = p_v + (2\sigma/3a_0)(G/G^* - 3)|\cos(\alpha_R - \beta)|,$$

while p_L^m is

$$p_L^m = p_v + \frac{2\sigma}{3a_0}\left(\frac{G}{G^*}\frac{a_0^2}{a_m^2} - 3\right)\frac{a_0}{a_m}|\cos(\alpha_R - \beta)|.$$

The condition $p_L^A < p_L^m$ is equivalent to

$$\left(1 - \frac{a_0}{a_m}\right)\left[3 - \frac{G}{G^*}\left(1 + \frac{a_0}{a_m} + \frac{a_0^2}{a_m^2}\right)\right] > 0.$$

Since $a_0 < a_m$, the first factor is positive while the second one, in general, can be positive or negative. However, the first nucleation threshold is given by p_L^A only if $G < G^*$, and in this case the second factor is readily seen to be positive also so that the inequality is satisfied.

Similarly, the expression (69) for p_L^B may be written

$$p_L^B = p_v - (4\sigma/3a_0)(3G^*/G)^{1/2}|\cos(\alpha_R - \beta)|.$$

Now, the condition $p_L^B < p_L^m$ can be shown to be equivalent to

$$Y^3 - Y + \tfrac{2}{3} > 0,$$

where

$$Y = (3G/G^*)^{1/2}a_0/a_m,$$

which is satisfied because the cubic is positive for $Y > 0$.

[1]M. Gernez, Philos. Mag. **33**, 479–481 (1867).
[2]C. Tomlinson, Philos. Mag. **34**, 136–143 (1867).
[3]C. Tomlinson, Philos. Mag. **34**, 229–230 (1867).
[4]R. B. Dean, J. Appl. Phys. **15**, 446–451 (1944).
[5]M. Kornfeld and L. Suvorov, J. Appl. Phys. **15**, 495–506 (1944).
[6]E. N. Harvey, D. K. Barnes, W. D. McElroy, A. H. Whiteley, D. C. Pease, and K. W. Cooper, J. Cell. Comp. Physiol. **24**, 1–22 (1944).
[7]H. B. Briggs, J. B. Johnson, and W. P. Mason, J. Acoust. Soc. Am. **19**, 664–677 (1947).
[8]F. G. Blake, Technical Memorandum No. 9, Acoustic Research Laboratory, Harvard University, Cambridge, MA (1949).
[9]F. G. Blake, Technical Memorandum No. 12, Acoustic Research Laboratory, Harvard University, Cambridge, MA (1949).
[10]L. J. Briggs, J. Appl. Phys. **21**, 721–722 (1950).
[11]W. Connolly and F. E. Fox, J. Acoust. Soc. Am. **26**, 843–848 (1954).
[12]W. J. Galloway, J. Acoust. Soc. Am. **26**, 849–857 (1954).
[13]F. E. Fox and K. F. Herzfeld, J. Acoust. Soc. Am. **26**, 984–989 (1954).
[14]F. Seitz, Phys. Fluids **1**, 2–13 (1958).
[15]D. Lieberman, Phys. Fluids **2**, 466–468 (1959).
[16]M. Strasberg, J. Acoust. Soc. Am. **31**, 163–176 (1959).
[17]D. Sette and F. Wanderlingh, Phys. Rev. **125**, 409–417 (1962).
[18]V. A. Akulichev, Sov. Phys. Acoust. **12**, 144–149 (1966).
[19]M. Greenspan and C. E. Tschiegg, J. Res. Natl. Bur. Stand. **71C**, 299–311 (1967).
[20]R. E. Apfel, J. Acoust. Soc. Am. **48**, 1179–1186 (1970).
[21]M. G. Sirotyuk, Sov. Phys. Acoust. **16**, 237–240 (1970).
[22]A. T. J. Hayward, J. Phys. D **3**, 574–579 (1970).
[23]R. H. S. Winterton, J. Phys. D **10**, 2041–2056 (1977).
[24]C. A. Ward, A. Balakrishnan, and F. C. Hooper, J. Basic Eng. **92**, 695–704 (1970).
[25]L. A. Crum, Nature **278**, 148–149 (1979).
[26]D. E. Yount, J. Acoust. Soc. Am. **65**, 1429–1439 (1979).
[27]D. E. Yount, J. Acoust. Soc. Am. **71**, 1473–1481 (1982).
[28]C. A. Ward, W. R. Johnson, R. D. Venter, S. Ho, T. W. Forest, and W. D. Fraser, J. Appl. Phys. **54**, 1833–1843 (1983).
[29]D. E. Yount, J. Acoust. Soc. Am. **76**, 1511–1521 (1984).
[30]R. A. Roy, A. A. Atchley, L. A. Crum, J. B. Fowlkes, and J. J. Reidy, J. Acoust. Soc. Am. **78**, 1799–1805 (1985).
[31]P. S. Epstein and M. S. Plesset, J. Chem. Phys. **18**, 1505–1509 (1950).